



HAL
open science

East Australian cyclones and air-sea feedbacks

Guillaume Sérazin, A. Di Luca, A. Sen Gupta, Marine Rogé, Nicolas Jourdain, D. Argüeso, C. y S Bull

► **To cite this version:**

Guillaume Sérazin, A. Di Luca, A. Sen Gupta, Marine Rogé, Nicolas Jourdain, et al.. East Australian cyclones and air-sea feedbacks. *Journal of Geophysical Research: Atmospheres*, 2021, 126 (20), pp.e2020JD034391. 10.1029/2020JD034391 . hal-03456203

HAL Id: hal-03456203

<https://hal.science/hal-03456203v1>

Submitted on 29 Nov 2021

HAL is a multi-disciplinary open access archive for the deposit and dissemination of scientific research documents, whether they are published or not. The documents may come from teaching and research institutions in France or abroad, or from public or private research centers.

L'archive ouverte pluridisciplinaire **HAL**, est destinée au dépôt et à la diffusion de documents scientifiques de niveau recherche, publiés ou non, émanant des établissements d'enseignement et de recherche français ou étrangers, des laboratoires publics ou privés.

East Australian cyclones and air-sea feedbacks

G. Sérazin^{1,2}, A. Di Luca^{1,2}, A. Sen Gupta^{1,2}, Marine Rogé^{1,2}, N. C. Jourdain³, D. Argüeso⁴, C. Y. S. Bull⁵

¹Climate Change Research Centre, University of New South Wales, Sydney, Australia

²ARC Centre of Excellence for Climate Extremes, University of New South Wales, Sydney, Australia

³Univ. Grenoble Alpes/CNRS/IRD/G-INP, IGE, Grenoble, France

⁴Physics Department, University of the Balearic Islands, Palma, Spain

⁵Department of Geography and Environmental Sciences, Northumbria University, Newcastle upon Tyne, UK

Key Points:

- High-resolution regional coupled modelling can simulate key features of East Australian cyclones
- Cyclone intensity is sensitive to mechanical and thermal air-sea feedbacks at mesoscales
- Coupled and atmosphere-only models mainly differ in simulating cyclone properties north of 30°S

Corresponding author: Guillaume Sérazin, serazing@gmail.com

Abstract

The importance of resolving mesoscale air-sea interactions to represent cyclones impacting the East Coast of Australia, the so-called East Coast Lows (ECLs), is investigated using the Australian Regional Coupled Model based on NEMO-OASIS-WRF (NOW) at $1/4^\circ$ resolution. The fully coupled model is shown to be capable of reproducing correctly relevant features such as the seasonality, spatial distribution and intensity of ECLs while it partially resolves mesoscale processes, such as air-sea feedbacks over ocean eddies and fronts. The mesoscale thermal feedback (TFB) and the current feedback (CFB) are shown to influence the intensity of northern ECLs (north of $30^\circ S$), with the TFB modulating the pre-storm sea surface temperature by shifting ECL locations eastwards and the CFB modulating the wind stress. By fully uncoupling the atmospheric model of NOW, the intensity of northern ECLs is increased due to the absence of the cold wake that provides a negative feedback to the cyclone. The number of ECLs might also be affected by the air-sea feedbacks but large interannual variability hampers significant results with short term simulations. The TFB and CFB modify the climatology of sea surface temperature (mean and variability) but no direct link is found between these changes and those noticed in ECL properties. These results show that the representation of ECLs, mainly north of $30^\circ S$, depend on how air-sea feedbacks are simulated. This is particularly important for atmospheric downscaling of climate projections as small-scale sea surface temperature interactions and the effects of ocean currents are not accounted for.

Plain Language Summary

Air-sea interactions occur at a variety of spatial scales, including those of the size of ocean eddies. Such interactions are partially resolved in the Australian Regional Coupled Model used to simulate the cyclones impacting the East Coast of Australia, the so-called East Coast Lows (ECLs). The effect of different feedbacks between the ocean and the atmosphere, including those due to mechanical and thermal exchanges over ocean eddies, are tested on the properties of ECLs. Significant effects are found on the intensity of ECLs north of $30^\circ S$, with also potential effects on the number of ECLs. The air-sea feedbacks modify the climatology of sea surface temperature, with no direct link to ECL changes. Such experiments eventually demonstrate that small-scale air-sea feedbacks may matter for representing current Australian climate and its change in the future.

1 Introduction

The east coast of Australia is particularly impacted by low-pressure systems, locally known as East Coast Lows (ECLs), that strongly affect human activities as they can induce severe damage resulting from strong winds, major floods due to heavy rainfalls, and coastal erosion linked to storm surges and large swell (Short & Trenaman, 1992; Dowdy et al., 2014, 2019). Despite these negative impacts on human populations and infrastructure, ECLs are also an essential source of rain and water for natural and artificial reservoirs (A. S. Pepler, Coutts-Smith, & Timbal, 2014).

ECL is a general term that includes a variety of low-pressure weather systems over the South West Pacific ocean, ranging from warm core barotropic tropical cyclones to cold core baroclinic extratropical cyclones, with a substantial proportion of hybrid cyclones, having a warm core in the lower troposphere and a cold core in the upper troposphere (Cavicchia et al., 2019, 2020). Depending on their vertical thermal structure (Hart, 2003), cyclones may extract their energy from diabatic heating at the surface to feed convection, and by converting available potential energy into kinetic energy through baroclinic instabilities.

The simulation of ECLs is often examined in high-resolution atmospheric models subject to prescribed sea surface temperatures (SSTs) or in coarse global climate models that do not include small-scale air-sea interactions (e.g., Dowdy et al., 2014; A. S. Pepler, Di Luca, et al., 2016; Di Luca et al., 2016). However, there is growing evidence that air-sea interactions occurring at scales of oceanic mesoscale eddies $\mathcal{O}(10\text{-}100\text{ km})$ account for a significant amount of thermal and mechanical energy exchanges between the ocean and the atmosphere (e.g., Small et al., 2008; Chelton & Xie, 2010; Frenger et al., 2013; Renault, Molemaker, McWilliams, et al., 2016; Renault et al., 2019). Including a high-resolution dynamical ocean component in climate models may therefore help to better represent air-sea feedbacks and could potentially improve the simulation of atmospheric phenomena including cyclones. Two types of mesoscale feedbacks are usually distinguished (Renault et al., 2019): (1) a mechanical feedback induced by the surface oceanic currents, the so-called current feedback (CFB), (2) a thermal feedback (TFB) induced by the impact that small-scale SST structures have on the atmosphere.

The CFB modulates local surface wind stress by adding or subtracting momentum from the atmospheric winds. The averaged effect of the CFB is a net modification of the wind stress curl and wind vorticity, rather than a modification of the averaged wind stress amplitude or wind velocity (Renault et al., 2019). CFB-induced changes in the wind stress curl drive small-scale anomalies in Ekman pumping, resulting in a slow down of ocean currents and a dampening of ocean eddy kinetic energy, estimated to be around 30% on average over the global ocean (Jullien et al., 2020). Therefore, the CFB results in a net loss of mechanical energy in the ocean and a net gain to the atmosphere. As wind velocities are generally much larger than ocean currents, especially the winds associated with storms such as ECLs, one may expect that the amount of mechanical energy saved by the atmosphere would only cause a small relative acceleration of atmospheric winds. Moreover, the CFB may have additional effects on the mean SST as it modifies the position, the stability and the transport of western boundary currents (Renault, Molemaker, Gula, et al., 2016; Renault et al., 2017), with a likely change to the associated SST fronts and water masses. In the context of this study, we might expect SSTs in the East Australian Current to be affected by the CFB. This could modulate ECL activity through, for example, a modification of the land-sea temperature contrast (McInnes et al., 1992; A. S. Pepler, Alexander, et al., 2016).

Whilst the ocean variability is primarily forced at large scales by the atmosphere (Bishop et al., 2017; Small et al., 2020), with positive anomalies of surface wind stress inducing a cooling of the ocean through latent and sensible heat fluxes, the opposite behaviour has been described at mesoscales, and is associated with the TFB. Small-scale warm SST anomalies have been associated with positive anomalies in the surface wind stress in satellite observations (Xie, 2004), which supports the fact that the ocean forces the atmosphere at mesoscales. Through changes in surface turbulent heat fluxes, the TFB modifies the stability of the atmospheric boundary layer (ABL) that modulates momentum transfer from the top to the bottom of the ABL resulting in a rectification of air-sea exchanges (see Small et al. (2008) and Oerder et al. (2016) for details on the physical mechanisms involved). The impacts of small-scale SST anomalies can extend beyond the atmospheric boundary layer with notable effects on the large-scale circulation of the troposphere and on atmospheric storm tracks (e.g., Piazza et al., 2016; Ma, Chang, et al., 2016). Mesoscale ocean eddies and fronts may be responsible for moist diabatic processes (Willison et al., 2013; Zhang et al., 2019) and may influence atmospheric convection (Smirnov et al., 2014), affecting clouds and rainfall (Frenger et al., 2013). More specific to Australian climate, warm core eddies in the East Australian Current (EAC) region were shown to influence the location of thunderstorms and peak rainfall associated with specific intense ECL events (Chambers et al., 2014, 2015), albeit with no significant change in the ECL wind intensity.

Another feedback that generally concerns tropical cyclones is the cyclone-induced cooling at the upper ocean that reduces the cyclone’s maximum potential intensity (Emanuel, 1999). This negative feedback reduces the amount of latent heat provided to the cyclone with the ocean surface cooling mainly caused by oceanic vertical mixing, advection and air-sea exchanges (e.g., Vincent et al., 2012). While the storm-induced SST cooling has synoptic scales, ocean mesoscale eddies have been shown to influence the surface cooling by enhancing or preventing storm-induced upwelling and mixing (Jullien et al., 2014). This negative feedback might apply to ECL occurring in the subtropics north of $30^{\circ}S$ since their dynamical characteristics get closer to those of tropical cyclones with warm core or hybrid structures (Cavicchia et al., 2019).

Following those aforementioned studies, we hypothesise that air-sea feedbacks, including those occurring at mesoscales, can modify the thermal and baroclinic sources of energy that feed ECLs (Cavicchia et al., 2019). They are likely to do so by directly impacting the life cycle of ECLs, or by modifying the average ocean SST. In this study, we thus investigate to what extent a dynamical atmosphere-ocean model, that partially resolves mesoscale ocean eddies and fronts, can modify the simulation of ECLs due to air-sea feedbacks. We focus on three main questions:

1. Is a regional coupled model (RCM), including mesoscale feedbacks, capable of representing the distribution and intensity of ECLs?
2. Are ECL properties sensitive to change in mesoscale air-sea feedbacks (i.e., CFB and TFB)?
3. Are ECLs significantly modified by fully removing coupled air-sea feedbacks (as is the case in a standalone atmospheric model), while preserving the small-scale SST information at the ocean boundary?

To address the first question, ECL statistics in a reference hindcast experiment are compared with those from a reanalysis dataset considered as an observational reference. To address the second question, we perform a hierarchy of numerical experiments to isolate the effects of the CFB and of the TFB on the representation of ECLs. To address the final question, we compare the representation of ECLs in this coupled system with a standalone atmospheric model forced by the same prescribed SST field. These questions will help to address the broader issue of the costs and benefits of using high-resolution RCM for climate projections compared to using standalone atmospheric models for regional atmospheric downscaling (Hewitt et al., 2017).

This study is organised as follows. Section 2 describes the RCM and the standalone atmospheric model used as well as the sensitivity experiments performed to isolate the different air-sea feedbacks. Methods for tracking ECLs and the observational reference are also described in this section. Section 3 compares the ECL and SST climatologies between the fully-coupled simulation and an atmospheric reanalysis. Section 4 shows how different air-sea feedbacks impact on ECL and SST climatologies. Section 5 isolates common events between the reference simulation and each of the sensitivity simulations to study the impact of air-sea feedbacks on the life cycle of ECLs. Section 6 summarises our results and discusses the added value of accurately representing air-sea feedbacks in a RCM for climate projections around Australia.

2 Data and methods

2.1 Regional coupled model and experiments

The NEMO-OASIS-WRF (NOW) ocean-atmosphere coupled regional model, developed by Samson et al. (2014) is applied over the CORDEX (Coordinated Regional Climate Downscaling Experiment) Australasian domain (covering Indonesia, Australia, New Zealand, and the South-Western Pacific, Figure 1a). Oceanic and atmospheric compo-

nents are the NEMOv3.4 (Madec, 2008) and the WRFv3.5.1 (Skamarock et al., 2008) models, respectively. Both components interact through the OASIS3-MCT2 coupler (Valcke, 2013), sending SST and surface ocean currents from the ocean to the atmosphere. Wind stress, heat fluxes (sensible, latent, longwave and shortwave radiation) and freshwater fluxes (precipitation minus evaporation) are computed within the atmospheric model and sent back through OASIS to the ocean model. By default, the turbulent fluxes are computed based on relative winds (wind velocity minus surface ocean velocity) and take into account the impact of ocean currents on the atmospheric boundary layer (Lemarié, 2015; Oerder et al., 2016). The coupling is done every hour and therefore includes the effect of the diurnal cycle. This model configuration is identical to the one described by Bull et al. (2020), including the physical parameterisations used, which are briefly summarised below. For practical purposes, WRF and NEMO are run on the same $1/4^\circ$ horizontal grid (Arakawa C-grid) corresponding to an average grid spacing of 24 km. As pointed out by Jullien et al. (2020), the $1/4^\circ$ resolution underestimates ocean mesoscale activity and the associated CFB. However, the $1/4^\circ$ resolution is computationally more affordable for running multiple experiments and is of broad interest as it corresponds to the resolution of several high-resolution global coupled models in the latest Coupled Model Intercomparison Project, i.e. CMIP6. The different simulations performed with the NOW model are summarised in Figure 1b and are described below. Note that all the simulations are run over the same period (i.e., 1989-2009) but the first spin-up year will be removed from the analyses.

The ocean component NEMO has 75 vertical levels on z -coordinates and uses partial cells to process the bathymetry (Barnier et al., 2006). It uses a momentum advection scheme that conserves energy and enstrophy (Penduff et al., 2007; Le Sommer et al., 2009), a total variance diminishing tracer advection scheme, an isopycnal Laplacian tracer diffusion operator, a vertical mixing scheme based on the turbulent kinetic energy closure model (Blanke & Delecluse, 1993).

The atmospheric component WRF uses 45 terrain-following pressure levels. Convective processes are represented using the Betts-Miller-Janjić scheme (Janjić, 1994). Other physical parameterisations include: the WRF single-moment three-class microphysics scheme (WSM3; Hong et al., 2004), a simple cloud-interactive shortwave radiation scheme (Dudhia, 1989), the Rapid Radiation Transfer Model (RRTM) for longwave radiation (Mlawer et al., 1997), the WRF simple five-layer (thermal diffusion) land surface model. No spectral nudging was used within the WRF model, which implies that each simulation will develop its own internal variability, while the forced variability will be conditioned by the same ocean and atmosphere boundary conditions.

2.1.1 Fully coupled control experiment (NOW-CTRL)

The control experiment, NOW-CTRL (Figure 1b), consists of running the fully coupled NOW model over the period 1989-2009. The atmospheric model is driven at the boundaries by 6-hourly atmospheric fields from the ERA-Interim reanalysis (Dee et al., 2011), including wind velocity, potential temperature, specific humidity and geopotential height. The oceanic model is forced at the lateral boundaries with ocean velocities, potential temperature and practical salinity coming from the ORCA025-L75-MJM95 simulation (Barnier et al., 2011), a global ocean simulation driven by ERA-Interim surface forcing. The NOW-CTRL experiment is a hindcast and is a benchmark simulation attempting to reproduce the climate over and around Australia over two decades. This NOW-CTRL experiment corresponds to the HIST experiment analysed in Bull et al. (2020).

2.1.2 Suppression of the ocean current feedback (NOW-NoCFB)

A simulation named NOW-NoCFB (Figure 1b) is designed to suppress the dynamical feedback due to ocean currents (Renault, Molemaker, McWilliams, et al., 2016), in

the computation of the wind stress and the heat fluxes. To do so, the ocean current velocity sent to the atmospheric model are set to zero. The atmospheric model therefore computes the air-sea exchanges with only the absolute wind velocity and sends these wind stress and heat fluxes back to the ocean model.

2.1.3 *Suppression of the mesoscale thermal feedback (NOW-NoTFB)*

A simulation named NOW-NoTFB (Figure 1b) aims at testing the effect of the TFB due to mesoscale ocean structures by suppressing the small-scale SST anomalies in the air-sea coupling. This is achieved by smoothing the SST using an on-the-fly Gaussian filter, whose weights are applied by the OASIS coupler. Consistently with the study of Renault et al. (2019), we use a standard deviation of 4 grid points estimated on a 25×25 ($6\sigma + 1 \times 6\sigma + 1$) window with values set to 0 outside the $6\sigma + 1$ circle. The resulting filter cutoff is about 250 km. The filter weights close to the coast are normalised to take into account only ocean values. The filter is designed to remove only mesoscale features, but other studies have used larger cutoff and even anisotropic filters that can remove more physical processes (e.g. Ma, Chang, et al., 2016; Ma, Jing, et al., 2016). The filter presented here preserves SST anomalies at synoptic scales such as cold wakes under tropical cyclones. Similar filter cutoffs have also been used to isolate mesoscale variability from the large-scale variability (Sérazin et al., 2014). This filter is only applied from the ocean to the atmosphere, and only for SST (i.e. the atmosphere does not feel any mesoscale SST variability).

2.2 Regional standalone atmospheric model

ECLs are commonly simulated using standalone atmospheric models, which dynamically downscale current or future climate information from the boundaries. This approach is represented here with the atmosphere-only component of the NOW modelling system (i.e., WRF) forced with prescribed SST. For consistency, the SST field is taken from 6 hourly outputs (snapshots) of the fully-coupled simulation NOW-CTRL. This simulation is termed WRF-ONLY (Figure 1b) hereafter.

The interaction with the ocean differs in three aspects compared to the fully coupled NOW model (i.e. NOW-CTRL, NOW-NoCFB, NOW-NoTFB). First, the SST is prescribed, the ocean surface will not be able to adapt to the diverging atmospheric solution of WRF-ONLY. Secondly, the forcing is done every 6 hours, which subsamples the diurnal cycle, while the coupling is done every hour in the NOW model. Finally, the ocean currents are not used to force the atmospheric model as their effects are generally considered to be small on atmospheric winds in standalone atmospheric simulations. This assumption will be partially addressed in the coupled framework with the NOW-NoCFB simulation, but further simulations will be required to assess the importance of ocean currents such as running a standalone atmospheric model with relative winds, potentially using coupling coefficients (e.g., Renault et al., 2020; Jullien et al., 2020). Such simulations are left for future work.

2.3 Observational reference

While our regional model is driven by ERA-Interim at the lateral boundaries, we use the fifth global reanalysis ERA5 (Hersbach et al., 2020) over the period 1990-2009 as an observational reference. ERA5 is the product of a 4D-var data assimilation scheme based on the ECMWF’s Integrated Forecast System run with 137 hybrid sigma/pressure levels and a horizontal spatial resolution of 31 km (0.28°). ERA5 outputs are available globally on a regular latitude-longitude $0.25^\circ \times 0.25^\circ$ grid with a temporal resolution of 1 hour. The SST used in ERA5 to force the model comes from HadISST2.1.1.0 (Rayner et al., 2003) between January 1989 and August 2007 on a $0.25^\circ \times 0.25^\circ$ grid. After this period the OSTIA product (Donlon et al., 2012) is used with a higher resolution grid ($0.05^\circ \times 0.05^\circ$).

Although ERA-Interim is used at the boundaries to force the NOW model, we prefer using ERA5 data as the spatial resolution is finer than ERA-Interim and is close to the NOW model. For comparison purposes, the SST from ERA5 is regridded onto the NOW grid using a conservative method.

2.4 Identifying and tracking of ECLs

In order to identify ECLs around the Australian East Coast, we use the same pressure gradient method to detect low pressure systems as Di Luca et al. (2015), who adapted this method from Browning and Goodwin (2013). Lows are identified by searching for both a local minimum in the mean sea level pressure (MSLP) field and a MSLP gradient around the local minimum that exceeds a given threshold. The pressure gradient value is computed by averaging differences between the minimum MSLP and the values in grid points located within a radius of 300 km around the central pressure. The value of the 300-km MSLP gradient mean threshold was chosen to be 5.4 hPa, larger than used in previous studies, but suited to focus on the more intense ECLs that are more likely to interact with the ocean. The search is restricted to the latitudes between 10 and 55°S and longitudes between 135 and 172 °E that correspond to the tracking domain (Figure 1a).

Once lows have been detected for individual time steps, cyclone tracks are generated by grouping lows that are close in time and space. Only lows that pass over the analysis region (i.e., spend at least one time step) are retained. The analysis region encompasses the area between 40 and 20°S and between 150 and 165°E (Figure 1a) and is thus very similar to the region used in other studies looking at ECLs (e.g., Di Luca et al., 2015; A. S. Pepler, Alexander, et al., 2016; Cavicchia et al., 2019). Tracks are constructed by a nearest neighbour search in the following 6-hourly MSLP field around a cyclone position. The search extends to a maximum distance of 750 km assuming that a cyclone does not move faster than 125 km h⁻¹. In the case that two different lows are found within a distance of 300 km, only the more intense low is retained. A number of lows appear to be quasi-stationary features that might be associated either with heat lows or with uncertainties in extrapolating the atmospheric pressure to mean sea level. In this analysis, we filter out some of these quasi-stationary systems by discarding cyclones that move at an average speed less than 5 km h⁻¹ over the total duration of the event. For this analysis we only retain events that last at least three consecutive 6-hourly time steps and all statistics are computed in the tracking region in order to include the life cycle of ECL events. A. S. Pepler, Di Luca, et al. (2014) compared this pressure gradient method to two other ECL identification methods based on the Laplacian of MSLP (e.g., Lim & Simmonds, 2002; A. Pepler & Coutts-Smith, 2013) and on the upper-level geostrophic vorticity (e.g., Dowdy et al., 2012, 2013). They concluded that the three methods gave similar results for extreme ECL events, including those with explosive developments.

The non-parametric bootstrap method is used to evaluate the errors made on the mean values due to the use of a finite set of ECL samples. The data is randomly resampled with replacement to build a new set of ECL samples from which the mean is estimated. This process is reiterated a sufficient number of times - in this study, we use 1000 samples - to build a probability density function of the error on the mean estimates. Confidence intervals are then defined relative to this probability density function.

2.5 Classification of East Coast Lows

The cyclone systems impacting the east coast of Australia are identified within the box 135°E-172°E / 50°S-10°S by the pressure gradient tracking, and are separated into two distinct categories based on a latitude cutoff (Figure 1a). By convention, cyclones north of 30°S will be termed northern ECLs (NECLs), whereas ECLs south of 30°S will be referred as southern ECLs (SECLs). Since some cyclones can move from one box to

the other, their occurrences will be split between the two categories in the results. Unlike Cavicchia et al. (2019), this classification is not based on physical features, but it is well suited to illustrate the contrasting response of cyclones to air-sea coupling depending on their latitude range. Following A. S. Pepler, Di Luca, et al. (2016), we additionally differentiate ECLs occurring during the cool season (May-October) from those occurring during the warm season (November-April).

North of $30^{\circ}S$, NECLs principally include (i) proper tropical cyclones that extract most of their energy from a warm upper ocean, (ii) ex-tropical cyclones that migrate southwards and derive from tropical cyclones, (iii) easterly trough lows that develop along the eastern seaboard between moist subtropical easterlies and cold air over the Australian mainland, and (iv) inland troughs that develop over land west of the Great Dividing Range (Browning & Goodwin, 2013). During the warm season, NECLs mainly develop either with a warm core, characteristic of tropical cyclones, or with a hybrid structure (lower warm core and upper cold core) (Cavicchia et al., 2019). As for tropical cyclones, hybrid cyclones extract their energy from diabatic heating at the ocean surface.

South of $30^{\circ}S$, SECLs include (i) continental lows similar to inland troughs that evolve over the southern part of Australia and (ii) southern secondary lows that correspond to cyclones developing over the Southern Ocean, moving equatorward to eventually find warmer and moister conditions over the Tasman Sea (Browning & Goodwin, 2013). SECLs consists of cold core and hybrid cyclones that are more frequent during the cool season (Cavicchia et al., 2019; Quinting et al., 2019).

2.6 Matching ECLs across simulations

To allow the comparison of events that are common to two different simulations, such as those whose generation is initiated by common boundary forcing, we impose criteria to find pairs of events. Given an ECL occurrence i in the reference dataset, we look for all the ECL occurrences j in the second dataset that meet the following conditions:

- the distance δ_{ij} between the centres of the ECL occurrences i and j is less than Δx ,
- the time difference τ_{ij} between the ECL occurrences i and j is less than Δt ,

where Δx and Δt are chosen to be 600 km and 24 hours, respectively. Several occurrences j may meet both conditions simultaneously, including multiple occurrences belonging to the same ECL event. Once minimised, this score will give a single ECL occurrence j that most closely follows the ECL occurrence i from the reference dataset. The score is defined as follows:

$$score = \sqrt{\frac{\delta_{ij}^2}{\Delta x^2} + \frac{\tau_{ij}^2}{\Delta t^2}}. \quad (1)$$

Minimising this score gives pairs of ECL occurrences, from which we retrieve couples of ECL events by matching occurrences with their corresponding events. This process sometimes gives duplicated ECL pairs, that are filtered out to retain only unique ECL couples.

3 Model assessment

3.1 Number and intensity of ECLs

In a comparison with the ERA5 reanalysis, NOW-CTRL significantly overestimates the number of ECL events per year (Figure 2a and Figure 2b). This overestimate is primarily due to many more ECLs during the warm season, while the number of winter ECLs is more similar between the model outputs and ERA5. South of $30^{\circ}S$, the difference with

ERA5 in the number of warm-season ECLs is not as large as north of $30^{\circ}S$ but this difference remains statistically significant.

The meridional distribution of ECL days, i.e., the number of ECL days per bins of latitude during the period 1990-2009, is similar between NOW-CTRL (grey) and ERA5 (orange) during the cool season (Figure 2c). During this same cool season, ECLs are concentrated in the Tasman sea around $38^{\circ}S$ and $163^{\circ}E$ (Figure 3a), and are slightly shifted eastwards by a few degrees compared to ERA5 (Figure 3b), with also an increased probability of events occurring closer to the coast in NOW-CTRL. The warm season (Figure 2d), however, is strongly biased with an overestimated number of ECL days everywhere north of $39^{\circ}S$ in NOW-CTRL, with a maximum bias in the tropics between $24^{\circ}S$ and $15^{\circ}S$ (i.e., 3 to 4 times more ECL days in NOW-CTRL). During the warm season, ECLs are concentrated in the Coral Sea, close to New Caledonia around $23^{\circ}S$ and $160^{\circ}E$ (Figure 3c), and has a similar eastward shift with ERA5 (Figure 3d) as during the cool season. The cyclone density is essentially concentrated north of $30^{\circ}S$ in NOW-CTRL while ERA5 shows a more important contribution from events south of $30^{\circ}S$ (Figure 3c-d). The meridional distribution is consistent with the overestimate of summer events shown in Figure 2a-b. Note that the spatial distributions shown in Figure 3 are probability density functions modelled using a Gaussian function; the actual distribution is noisy and complicates the interpretation of raw data.

The mean pressure gradient extending radially outwards across the cyclone significantly differs between NOW-CTRL and ERA5 for SECLs south of $30^{\circ}S$ during both cool and warm seasons (Figure 2e-f), with the mean pressure gradients being significantly smaller and with a reduction in the upper quartile. Note that these effects are much larger during the cool season. North of $30^{\circ}S$, NECLs have, however, similar intensity between NOW-CTRL and ERA5 during the warm season (Figure 2g). Note that NECL pressure gradients are not shown for the cool season as there are not enough events for inferring robust statistics.

In summary, the NOW model tends to generate too many cyclones during the warm season, especially in the tropics, but of similar intensity compared to ERA5. On the contrary, the number of cyclones are similar during the cool season, but the model tends to generate weaker events compared to ERA5. ECLs eventually tend to occur further east in the NOW model.

3.2 SST climatology

Since the SSTs affect the transfer of thermal energy and may influence atmospheric baroclinicity, any substantial differences in SSTs are likely to impact the climatology of ECLs. Here, we investigate modelled SST biases based on the NOW-CTRL experiment compared to ERA5 and we compare these biases with those in the ECL climatology.

South of $30^{\circ}S$, the effect of the EAC along the coast is recognisable as it transports warm tropical waters southwards along the Australian coast as shown by the NOW-CTRL SST in Figure 4a,e. The EAC bifurcates at around $32.5^{\circ}S$ (e.g., Oke et al., 2019) to separate into the Tasman front flowing eastwards up to the north of New Zealand and into the EAC extension flowing southwards along the coast of Tasmania, further prolonged by the Tasman leakage around Tasmania. The effect of these currents is evident in the standard deviation of daily SST shown in Figure 4c,g as they are hotspots of eddy and SST variability (see also Bull et al., 2017), intensified during the warm season. The SST variability is also intensified north of $30^{\circ}S$ over the Coral Sea during the warm season.

In the Tasman Sea and in the southern part of the Coral Sea, the NOW-CTRL experiment has a cool bias up to $1^{\circ}C$ compared to ERA5 (Figure 4b,f). The mean SST under the South Pacific Convergence Zone is positively biased (warmer) in NOW-CTRL (Figure 4b), associated with smaller SST variability (Figure 4d) during the cool season.

The NOW-CTRL experiment has larger SST variability in the Coral Sea and along the currents that forms the EAC system (Figure 4d,h). This larger variability is probably linked with different eddy kinetic energy that modulates local heat transport and SST fluctuations. South of Australia, NOW-CTRL has also a warm bias larger than 1°C , with a bias exceeding 2°C in the Tasman outflow, likely linked with a larger transport of the EAC extension and of the Tasman outflow in NOW-CTRL compared to observations (see the comparison of transports with observational estimates in Figure 2 of Bull et al. (2020)).

North of 30°S , having more NECL events in NOW-CTRL is not consistent with a cool bias in the mean SST compared to ERA5, except if cyclones are generated further north, i.e. under the South Pacific Convergence Zone where there is a warm bias. An increase in SST variability could also play a role in triggering more NECL events in this region. Other parameters in the NOW model could explain this bias in the number of NECL events, such as convective parameterisation, and will be discussed later in this study. Hence, the SST biases do not seem to be linked with the intensity of NECLs.

South of 30°S , the large biases in SST in the SECL region, be it on the mean or on the variability, do not seem to have an impact on the number of SECLs. However, the smaller intensity of ECL during the cool season in NOW-CTRL compared to ERA5 (Figure 2e) could be linked with a cooler Tasman sea or a warmer EAC extension and Tasman outflow.

4 Impact of air-sea feedbacks on ECL climatology

Even though there are some important differences between the characteristics of ECLs in the NOW simulations and observations, the model still provides a useful platform to examine the sensitivity of ECLs to small-scale air-sea coupling.

4.1 Number and intensity of ECLs

The number of NECLs is notably reduced during the warm season when air-sea feedbacks are partially or totally suppressed (Figure 5a). Removing the CFB effect has the biggest impact on the number of NECL events (18 % decrease), followed by the removal of the TFB (12 % decrease), then the full suppression of the ocean feedbacks with WRF-ONLY (7 % decrease). Error bars on the mean difference are estimated using a bootstrap method and show that the changes in NECL numbers are not significant at the 90% level due to large interannual variability on the 20 years of available data. However, a smaller confidence interval (e.g., at 85%) would make the changes due the TFB and CFB appear as significant (i.e., error bars not overlapping with 0).

While the suppression of either the TFB or the CFB impacts the number of NECLs, only the TFB has an impact on the number of SECLs, south of 30°S , with the largest effect occurring during the warm season (16 % decrease, Figure 5b). This difference is, however, not significant at the 90% level because of substantial interannual variability on these 20 years of data.

The number of ECLs during the cool season, including NECLs and SECLs, is barely impacted by the coupling (Figure 5a,b). Only a reduction in the number of ECL days is noticed between 35°S and 38°S on the meridional distribution shown in Figure 5c and is consistent between the three sensitivity experiments. During the cool season, the spatial distribution of ECL frequency is similar in NOW-NoCFB and WRF-ONLY (Figure 6a,c) compared to NOW-CTRL. Only the removal of the TFB induces a westward shift of the SECL location by a few degrees (i.e., from 163°E to 158°E , Figure 6b).

The meridional distribution of the number of ECL days during the warm season (Figure 5d) reflects the change in the number of NECLs noticed for the NOW-NoCFB simulation, with less occurrences between 15°S and 30°S . A reduction in the ECL oc-

currences is noticed south of $20^{\circ}S$ for NOW-NoTFB and WRF-ONLY, whereas these two simulations show increased occurrences north of this latitude. During the warm season, the spatial distribution of ECL frequency is stretched westwards (Figure 6d,f) in NOW-NoCFB and WRF-ONLY. In NOW-NoTFB, NECLs are shifted westwards and occur close to the Australian coast (Figure 6e) while they are concentrated on the other side of the analysis region in NOW-CTRL (Figure 3c), closer to New Caledonia.

Characteristics of NECLs do show robust changes. The mean intensity of NECLs, estimated by the pressure gradient (Figure 5g), is significantly increased in NOW-NoTFB and WRF-ONLY. In addition to affecting the mean intensity, the intensity of extreme NECL events (75% percentile) is also increased. These results suggest that ocean SST feedbacks damp or prevent the development of severe NECLs. A slight but significant reduction in the pressure gradient is noticed when the ocean currents seen by the atmospheric component are suppressed in NOW-NoCFB. The mean intensity of SECLs are not strongly affected by changes in the coupling in either seasons (Figure 5e-f).

4.2 SST climatology

To investigate why the ECL climatology is impacted by ocean feedbacks, we analyse the differences in the SST climatology and variability due to the TFB and the CFB. Removing either the CFB or the TFB may indeed modify the mean ocean state, including the mean SST, by affecting the wind stress and Ekman pumping. Warmer SSTs, such as a warmer EAC (A. S. Pepler, Di Luca, et al., 2014), could trigger more ECLs and induce an increase of ECL intensity. Warmer SSTs in the tropics are also expected to increase the intensity of ECLs behaving like tropical cyclones (e.g. Emanuel, 1999). The SST differences between the NOW sensitivity simulations and NOW-CTRL are shown in Figure 7 for the cool and warm seasons and for all the simulations, except for the WRF-ONLY simulation as the latter has the same mean SST as NOW-CTRL.

The suppression of the CFB induces a cooling of a few hundred kilometers along the EAC extension and extending to the Tasman leakage, particularly during the warm season (Figure 7a,e). In contrast, there is a warm anomaly at around $30^{\circ}S$ close to the Tasman front, where ocean eddy activity is generally high. This cold/warm dipole is possibly linked to changes in the transports of the EAC system because its dynamics may be impacted by the CFB, as found for other western boundary currents (Renault, Molemaker, Gula, et al., 2016; Renault et al., 2017). A slight warming is also noticed in the Coral Sea without the CFB. The suppression of the CFB has, however, a weak impact on the SST variability as no coherent patterns are distinguishable in Figure 7c,g.

The change in SST due to the TFB results in a complex pattern with fine scale structures due to the smoothing of mean SST fronts and large scale anomalies in regions where ocean eddies are ubiquitous (Figure 7b,f). North of its bifurcation point, the EAC temperature front is smoothed in NOW-NoTFB, which results in an artificial cooling along the coast compared to NOW-CTRL. This apparent cooling is linked to the EAC transporting warmer water than the surrounding water masses. South of $30^{\circ}S$, ocean eddies are numerous in the EAC system and their smoothing during the coupling exchange results in broad-scale warming. This same behaviour is also found east of Tasmania due to the eddies creating the Tasman leakage and the Tasman outflow. As mesoscale eddies are associated with substantial SST anomalies, the SST variability is strongly damped in NOW-NoTFB around the EAC detachment point, along the Tasman Front and along the Tasman Leakage (Figure 7d,h), with little difference between warm and cool seasons. In the Coral sea, the change in SST variability due to the TFB is usually small.

Overall, the changes in the SST climatology can only provide limited information about the change in the ECL climatology. South of $30^{\circ}S$, a substantial reduction in the SST variability along the EAC extension due to the suppression of the TFB could be a factor in the reduction in the number of SECLs, particularly by suppressing the effect

of the dominant warm core eddies present in this region. North of $30^{\circ}S$, we however expect only a weak influence related to changes in the mean SST and its variability on the NECL climatology (intensity and frequency) due to the TFB and CFB.

5 Impact of air-sea feedbacks on ECL life cycle

Because of changes in the climatology, such as changes in the mean SST as previously shown, the ECL cyclogenesis can be different between the experiments leading to more or less intense events. This point will be addressed later in the discussion as there is no clear index to quantify ECL cyclogenesis. The difference in the climatology of the ECL intensity can also be due to ECL events that are common in the experiments, but undergo different life cycles due to different air-sea feedbacks (TFB and CFB) or no feedback at all (WRF-ONLY). We focus here on this second point by matching ECL events between each sensitivity simulation and the NOW-CTRL simulation (see section 2.6 for the matching description) and compare the evolution and characteristics of only those common events.

5.1 Intensity of common ECL events

Comparison of the NOW-CTRL and NOW-NoCFB experiments show that the pressure gradient is not significantly modified by the suppression of the ocean current feedback south of $30^{\circ}S$ in either season (Figure 8a-b). This agrees with the previous results of Figure 5d-e where all the cyclone events were included. However, the suppression of the CFB tends to intensify the NECLs as the pressure gradient substantially increases (Figure 8c). This effect only becomes clear when common events are compared whereas the CFB have a smaller effect on the intensity when the full set is considered as in Figure 5g.

Removing the TFB also has a significant impact on NECLs by increasing the pressure gradient of common warm season events (Figure 8f). Unlike the case without the CFB, the TFB change for common events is consistent with the full set of cyclones shown in Figure 5g. Another noticeable impact is the reduction of the pressure gradient of SECLs during the warm season (Figure 8e), more pronounced when we consider only common events compared to the full distribution (Figure 5f). Finally, the TFB has no significant effect on SECL intensity during the cool season (Figure 8d).

Fully suppressing the coupling yields stronger NECL events by increasing the pressure gradients of common warm season events (Figure 8i), consistent with the full set of cyclones. Selecting only common events also shows that SECL events occurring during the cool season tend to be slightly, but significantly, more intense when the ocean coupling is fully suppressed (Figure 8g). This sensitivity to the full coupling does not show up when one considers the full set of events (Figure 5e).

5.2 Pre-storm ambient SST

The pre-storm ambient SST is taken here as the SST spatially averaged within a 200 km radius and temporally averaged between 10 and 5 days prior to the cyclone passing. The pre-storm ambient SST can modulate the potential thermal energy available for fuelling NECLs through latent and sensible heat such as for tropical cyclones (Bister & Emanuel, 1998; Emanuel, 1999).

In NOW-NoCFB, the pre-storm SST is not significantly different compared to similar events occurring in NOW-CTRL, while the pre-storm SST in NOW-NoTFB and WRF-ONLY is significantly larger by about $1^{\circ}C$ (Figure 9a). The increase in the pre-storm SST in NOW-NoTFB and WRF-ONLY is consistent with more intense events compared to common events in NOW-CTRL (Figure 8f,i), suggesting that air-sea feedbacks may

modulate the storm intensity through local changes in the SST. In WRF-ONLY, the SST difference with NOW-CTRL is explained by a significant shift of the mean cyclone latitude and longitude: common events tend to occur 1.3° further north and 1.3° further west on average in the uncoupled simulation (WRF-ONLY) as shown in Figure 9b. The change in the pre-storm SST in NOW-NoTFB is also linked to a westward shift of the mean cyclone longitude of 3.9° (Figure 9c). Note that the pairing method allows a maximum distance of 600 km between the centres of common events. Finally, the increase in NECL events in NOW-NoCFB cannot be explained by a change in the pre-storm SST. Note that no significant shifts in the latitude and longitude of the NECL centre is found for NOW-NoCFB. Note also that the eastward shift of common NECL events noticed for NOW-NoTFB and WRF-ONLY in Figure 9c is consistent with the cyclone distribution shown in Figure 6e,f.

The pre-storm SSTs were also computed for SECL events during cool and warm seasons and are shown in Figure S1 of Supplementary Information. We did not find any significant differences between the three sensitivity experiments and the NOW-CTRL experiment, suggesting that the significant differences in the SECL intensity shown in Figure 8e,g are not conditioned by the pre-storm SST despite the largest change in the climatological SST occurring south of 30°S . This suggests that convective processes do not play an important role in the development of SECLs compared to baroclinic processes that typically occur at these latitudes in the development of cold core cyclones (e.g., Cavicchia et al., 2019; Dowdy et al., 2019).

5.3 Air-sea exchanges under NECLs

Since air-sea feedbacks have the strongest impact on the intensity of NECLs during the warm season, we will focus on them here. During the passage of the storm, the upper ocean may interact with the atmosphere and modulate the storm characteristics. Here, we analyse the air-sea interactions relative to the pre-storm state (i.e average conditions between 10 and 5 days prior to the cyclone passing).

The mechanical exchanges between the atmosphere and the ocean are characterised here with the wind stress and results are shown in Figure 10a-c. The wind stress is retrieved from atmospheric outputs using

$$\|\tau\| = \rho_a u^{*2}, \quad (2)$$

where ρ_a is the air density and u^* is the friction velocity. The wind stress can be parameterised using the bulk formula

$$\tau = \rho_a C_D (\mathbf{U}_a - \mathbf{U}_o) \|\mathbf{U}_a - \mathbf{U}_o\|, \quad (3)$$

where C_D is the surface drag coefficient characterising the transfer of momentum, \mathbf{U}_a is the near-surface wind (lowest model level) and \mathbf{U}_o is the surface ocean current. The wind stress depends quadratically on the relative wind velocity $\mathbf{U}_a - \mathbf{U}_o$. In NOW-NoCFB, the wind stress does not include the effect of ocean currents \mathbf{U}_o (i.e, the CFB). Since the ocean circulation induced by the NECLs is cyclonic and tends to be aligned with the cyclone winds (Supplementary Information, Figure S2), atmospheric winds and ocean currents tend to compensate in NOW-CTRL, yielding a smaller wind stress on average compared to NOW-NoCFB (Figure 10a). In NOW-NoTFB and WRF-ONLY, the wind stress is larger than in NOW-CTRL because of the generally stronger near-surface wind speeds that are associated with stronger NECLs (Figure 10b,c). In WRF-ONLY, this increase in the wind stress may be further amplified by the absence of ocean currents in the wind stress calculation.

The passage of a NECL over the ocean induces a cooling of the SST (Figure 10p-r), generally known as a cold wake for tropical cyclones. Without the CFB, the SST cooling evolution is largely unaffected (Figure 10p). Conversely, without the TFB, the SST

cooling is significantly larger (Figure 10q). This change cannot be explained by an increased enthalpy flux from the ocean (Figure 10e), instead this cooling appears to be induced by enhanced vertical mixing penetrating deeper due to stronger wind stress (Supplementary Information, Figure S3) and is one of the main drivers of the cold wake of tropical cyclones (Vincent et al., 2012; Jullien et al., 2012).

The thermal exchanges are characterised by the enthalpy flux Q_H , that can be decomposed into the sum of a sensible heat flux Q_{SH} and a latent heat flux Q_{LH} , parameterised by the bulk formulae:

$$Q_{SH} = -\rho_a C_H C_p (\theta_a - \theta_o) \|\mathbf{U}_a - \mathbf{U}_o\|, \quad (4)$$

$$Q_{LH} = -\rho_a C_E L_v (q_a - q_o) \|\mathbf{U}_a - \mathbf{U}_o\|, \quad (5)$$

where C_H and C_E are surface bulk coefficients, C_p is the specific air heat capacity, L_v is the specific latent heat, θ_a and θ_o are respectively the temperature at the lowest atmospheric level and at the ocean surface, q_a and q_o are respectively the specific humidity at lowest atmospheric level and at the ocean surface. Note that both heat fluxes depend linearly on the relative wind velocity $\mathbf{U}_a - \mathbf{U}_o$. The enthalpy flux variations around the cyclone passing are not modified when the CFB is suppressed (Figure 10d), i.e. with $\mathbf{U}_o = \mathbf{0}$ in the computation of Q_{SH} and Q_{LH} ; both sensible and latent heat fluxes are not modified by the CFB (Figure 10g,j). This suggests that the CFB does not modulate the thermal exchanges under a NECL and only has a dynamical effect as noted earlier. Since $\|\mathbf{U}_a\| \gg \|\mathbf{U}_o\|$, sensible and latent heat fluxes only have a weak linear dependence to the ocean current velocity. An increase in the wind intensity, however, must be compensated by a decrease in the temperature and humidity difference between the air and the ocean surface to maintain similar enthalpy fluxes.

Similarly, the TFB does not alter the enthalpy flux variations induced by the NECL (Figure 10e). However, latent heat flux increases without the TFB (Figure 10h) as NECLs are stronger and generate larger wind speeds, while sensible heat flux decreases (Figure 10k) as a consequence of a cooler ocean surface θ_o (Figure 10q), that dominates over the increase in wind speed. Both latent and sensible heat fluxes compensate each other yielding similar enthalpy fluxes with and without the TFB.

When the atmosphere is simulated without any ocean feedbacks (i.e. WRF-only experiment), the enthalpy flux is increased, both through latent and sensible heat fluxes, during the passage of the cyclone and the next few days (Figure 10f,i,l). Contrary to the fully coupled simulation NOW-CTRL, a cold wake cannot develop under the cyclone in WRF-ONLY. Although cold anomalies are present at the ocean surface due to NECLs in NOW-CTRL, they are unlikely to collocate with NECLs in WRF-ONLY. Thus the energy extraction by the cyclone in WRF-ONLY is not diminished by the cooling of the ocean surface. The enthalpy flux, both through sensible and latent heat fluxes, keeps feeding the NECL.

Finally, we look at precipitation as it affects sea surface salinity and so upper ocean density and stratification. Precipitation increases in all three sensitivity experiments (Figure 10m-o), likely due to the increase in mean cyclone intensity noted previously. A fresh wake also develops under the cyclone as a likely consequence of increased precipitation that dilute sea surface salinity (Supplementary Information, Figure S3). This result contrasts with a salty wake that usually combines with a cold wake under tropical cyclones due to the vertical entrainment of saltier and colder water from the subsurface (Jourdain et al., 2013). However, NECLs are on average less intense than tropical cyclones with less efficient vertical mixing, so that the freshening effect of rainfall may become more important relatively (see the discussion in the appendix of (Jourdain et al., 2013)).

6 Conclusion and discussion

6.1 Discussion

While interannual variability was too large to make conclusive statements, our analysis suggested that air-sea feedbacks may impact the frequency of ECLs. These changes may relate to a number of different mechanisms, including large-scale changes in atmospheric circulation. To examine these we computed different indices that act as a proxy of ECL cyclogenesis. First, we examined differences in the strength of the subtropical ridge across simulations, which was shown to be negatively correlated to the ECL occurrence, based on minima of upper-tropospheric geostrophic vorticity (Dowdy et al., 2012). No clear impact of the air-sea coupling was found on the L-index (Drosowsky, 2005), which estimates the strength and position of the subtropical ridge (Supplementary Information, Figure S6).

As some ECL are tropical cyclones or ex-tropical cyclones, we also computed the index defined by Tippett et al. (2010) which has been designed to examine tropical cyclogenesis. This index is computed as an exponential polynomial including a dynamic contribution based on vorticity and vertical wind shear, and a thermal contribution based on sea surface temperature and relative humidity. Using this index, whose maps are shown in Figure S7 of Supplementary Information for each experiment, we found that tropical cyclones are expected to be slightly more frequent without the CFB between the Solomon islands and Vanuatu, and in the Gulf of Carpentaria. However, this result was not consistent with a tendency to have less NECLs without the CFB. Only the index computed for the NOW-NoTFB showed a slight reduction in tropical cyclone frequency consistent with less NECLs without the TFB.

We eventually computed the climatology of the cyclone potential intensity (Supplementary Information, Figures S8 and S9) on monthly timeseries and found that, on average, only the removal of the CFB is likely to increase the maximum winds by a few meters per second over the warm anomaly in the NOW-NoCFB simulation centred around $30^{\circ} S$, $160^{\circ} W$ (see Figure 7a). This could explain why NECLs are stronger without the CFB but this tendency is not corroborated by a warmer pre-storm SST (Figure 9). Removing the TFB only slightly changes the potential intensity locally over SST fronts. The potential intensity is almost similar in the atmosphere-only simulation suggesting that the intensity is mostly driven by the SST. The potential intensity theory is thus not able to predict that NECLs are more intense in the NOW-NoTFB and in the WRF-ONLY simulation.

By representing mesoscale feedbacks, the NOW model is able to represent some processes that might be important for the realistic simulation of ECLs. However, the NOW model contains substantial biases that need to be considered. In particular, NOW clearly overestimates the number of ECLs during the warm season, especially north of $30^{\circ} S$. A likely factor in contributing to this bias is the convective cumulus parameterisation (e.g. Dutheil et al., 2020). Lengaigne et al. (2019) show that different convective parameterisations can yield very different numbers of tropical cyclones in the NOW model when applied to the tropical Indian Ocean. Note that in NOW, the overestimate mostly occurs during the warm season, where the ocean surface is warmer and diabatic processes are likely to be more important for the formation and intensification of ECLs. Atmosphere-only simulations were performed using different cumulus schemes in the NARCLIM project (Evans et al., 2014). All simulations were shown to overestimate the number of ECL during the warm season compared to the atmospheric reanalyses used, with the Betts-Miller cumulus scheme yielding the largest overestimate (Di Luca et al., 2016). Investigating the impact of cumulus schemes in the NOW coupled model is certainly of interest to better understand model biases and will be tested in the future.

The current NOW model only partially resolves the mesoscale air-sea feedbacks as the resolution of the ocean grid is $1/4^\circ$. With this resolution, ocean eddies are weaker than observed and associated temperature fluctuations are also likely to be underestimated. Thus, our results likely provide a lower bound on estimates of the impact of mesoscale structures on the ECLs. In particular, the low sensitivity of SECLs to mesoscale feedbacks found in this paper might be due to the underestimate of ocean mesoscale activity with the $1/4^\circ$ resolution. To better represent air-sea feedbacks, one would need to increase resolution to about $1/12^\circ$ in the ocean model, but keeping a $1/4^\circ$ resolution for the atmospheric model is considered to be sufficient to correctly represent the effect of the CFB (Jullien et al., 2020).

Another important bias in the NOW model is a large warm SST bias south of Australia. Although this bias does not seem to impact on the number of SECLs it could be a factor in the underestimated SECL intensity bias south of $30^\circ S$. Since the air-sea feedbacks do not strongly impact on SECL intensity, correcting the SST bias might rather modify the atmospheric mean circulation and its baroclinicity leading to different SECL intensity. Performing a SST bias corrected experiment would help to investigate if it can improve the representation of SECL in the NOW model.

Using only one reanalyses as a reference for ECLs is certainly a limitation here, though the goal of this study was not to undergo a full assessment of the model performance but rather to experiment with air-sea feedbacks. A more detailed assessment of the model could be done by using additional reanalyses on their native grids such as the NCEP–DOE reanalysis 2 (Kanamitsu et al., 2002), the NASA Modern-Era Retrospective Analysis for Research and Applications (Rienecker et al., 2011) or the NCEP Coupled Forecast System Reanalysis (Saha et al., 2010) as done by Di Luca et al. (2015) to evaluate ECLs.

We chose to focus on large cyclonic systems by using a higher threshold (5.4 hPa / 300 km) compared to other studies (i.e., 1.8 hPa / 300, Di Luca et al., 2015, 2016; Brown-ing & Goodwin, 2013), because such systems would have a stronger impact on the ocean state and correspond to large intensity events that can be potentially destructive for human activities. We compared our results for two other thresholds: 1.8 hPa / 300 km and 3.6 hPa / 300 km. Results were qualitatively similar to the threshold used in the paper, except that the reduction in the number of northern ECLs due to air-sea feedbacks appears as significant with the smallest threshold (i.e., 1.8 hPa / 300 km) for all sensitivity simulations. However, this lower threshold is known to make an important number of false detections at high-resolution (Di Luca et al., 2015).

While the effective resolution of the WRF model is typically 5 to 7 times the grid (Skamarock et al., 2008), i.e., 120-168 km, the effective resolution of ERA5 remains unknown and should be clarified in the future. A close estimate is however provided by the ECMWF-IFS model at 25 km resolution whose effective resolution is shown to be around 125 km (Klaver et al., 2020; Roberts et al., 2020). Smoothing or regridding SLP fields could have been performed to homogenise the datasets at a coarser resolution, i.e., around 300 km, but (Di Luca et al., 2015) suggest that high-resolution sea level pressure fields are more appropriate to capture intense ECLs.

The additional cost of running the fully-coupled NOW model compared to the standalone WRF atmospheric model is affordable as the ocean model roughly represents 20% of the total computational time. In general, a standalone atmospheric model can be used to dynamically downscale future changes of ECL under global warming without including any ocean feedbacks, with the SST taken from coarse GCM outputs such as those produced for the Coupled Model Intercomparison Projects. However, such a strategy also lacks the small-scale SSTs in the forcing fields that could alter the representation of ECLs. The added value of the NOW model is thus to directly simulate these high-resolution SSTs under a changing climate as done in Bull et al. (2020).

6.2 Conclusion

In this study, we used the fully coupled regional ocean-atmosphere system NOW to examine cyclones over the South West Pacific and impacting the East Coast of Australia, i.e. ECLs, and compared these simulated ECLs with those from an atmospheric reanalysis. In particular, we investigated the sensitivity of ECLs to the small-scale oceanic features and their associated dynamical (CFB) and thermal (TFB) feedbacks. We also compared the representation of ECLs in this fully coupled model to those simulated by a standalone atmospheric model, as commonly used for downscaling climate projections.

Using ERA5 as an observational reference, we found that the current configuration of the NOW model is able to correctly generate some key features of the ECLs, such as the number of ECLs during the cool season (May-October) and the intensity of events during the warm season (November-April). However, NOW clearly overestimates the number of ECLs during the warm season, especially north of $30^{\circ}S$, where the ocean surface is typically cooler but more variable in NOW. ECLs also tend to occur further east in NOW. SST biases (mean and variability) in the ECL tracking region south $30^{\circ}S$ could also contribute to the underestimate in cyclone intensity noticed in NOW.

We demonstrated that removing mesoscale air-sea feedbacks (i.e., the TFB and the CFB) can impact on ECL intensity, particularly on common northern ECL (NECL, north of $30^{\circ}S$) events occurring across experiments during the warm season. Suppressing the TFB increases the pre-storm ambient SST by shifting ECL westwards close to the Australian coast and may therefore increase the maximum potential intensity of the NECLs, yielding more intense events. Without the TFB, the ocean surface cooling is also larger under northern cyclones, as a response to generally more intense events, and prevents the increase of the enthalpy flux. We found that the intensity of southern cyclones (SECL, south of $30^{\circ}S$) is also influenced by the TFB during the warm season, but to a lesser extent than NECLs. Suppressing the CFB also increases the wind stress of NECLs, likely due to a mechanical effect absent without the CFB: ocean currents induced by the NECL are aligned with the winds and negatively feedback with the wind stress.

Mesoscale air-sea feedbacks might also influence the number of ECL generated in the NOW model. South of $30^{\circ}S$, the TFB suppression alone reduced SECL numbers by 15% in summer but given the large interannual variability this change was not found to be statistically significant at the 90% level. North of $30^{\circ}S$, suppressing the TFB or the CFB showed summertime decreases in NECL numbers, but again the changes were not significant. Longer experiments are needed to verify whether or not mesoscale air-sea feedbacks have a significant impact on the number of ECLs. Our results also suggest that mesoscale air-sea feedbacks modify the ECL locations, by spreading and shifting the probability density function eastwards.

Finally, we found that fully suppressing air-sea coupling by using a standalone atmospheric model with the same SST mainly affects NECLs at low latitudes. NECLs are shifted northwards on average in the standalone atmospheric model so that the SST experienced by individual NECLs is generally warmer, which thereby provides more energy to the storm. By being able to represent the negative feedback of the cold wake under NECLs, the NOW climate models capture the correct NECL intensity while this feedback is absent in the standalone atmospheric model, which generates excessively large enthalpy fluxes at the ECL passes. We also note an impact of the coupling on SECL intensity during the cool season, but those changes remain unexplained by the analyses performed in this article: pre-storm SSTs, composite analysis (shown in Figure S1, S4 and S5 in Supplementary Information). Although NECLs are shifted northward, fully removing air-sea feedbacks does not impact significantly the total number of cyclones.

Acknowledgments

This research was supported by the Australian Research Council (ARC) Centre of Excellence for Climate Extremes (CE110001028). The NOW and WRF simulations were run using Computational resources provided by the NCI National Facility at the Australian National University, through awards under the Merit Allocation Scheme, the Intersect allocation scheme, and the UNSW HPC at NCI Scheme. Alex Sen Gupta acknowledges funding from the Australian Research Council (DP180101251, DP180100048, DP180102357). Daniel Argüeso was supported by the European Union’s REHIPRE project (H2020-MSCA-IF-2016-743547) and the COASTEPS project (CGL2017-82868-R MEIC/AEI/EU FEDER) financed by the Spanish Government and the EU FEDER funds. The scripts used to generate the NOW configuration and associated inputs are provided by Nicolas C. Jourdain (<http://doi.org/10.5281/zenodo.3760905>). The scripts used for the post-processing of NOW outputs are available (online DOI: 10.5281/zenodo.5121607).

References

- Barnier, B., Dussin, R., & Molines, J.-M. (2011). *ORCA025.L75-MJM95: Scientific Validation Report (ScVR) for V1 Reprocessed Analysis and Reanalysis* (Tech. Rep. No. MYO-WP04-ScCV-rea-CNRS.) Grenoble, France: CNRS-LEGI. Retrieved from https://www.drakkar-ocean.eu/publications/reports/ORCA025_JMJ95_MY0_ScVR-Re_An-LEGI.pdf
- Barnier, B., Madec, G., Penduff, T., Molines, J.-M., Treguier, A.-M., Le Sommer, J., ... de Cuevas, B. (2006, December). Impact of partial steps and momentum advection schemes in a global ocean circulation model at eddy-permitting resolution. *Ocean Dynamics*, *56*(5-6), 543–567. doi: 10.1007/s10236-006-0082-1
- Bishop, S. P., Small, R. J., Bryan, F. O., & Tomas, R. A. (2017, October). Scale Dependence of Midlatitude Air–Sea Interaction. *Journal of Climate*, *30*(20), 8207–8221. Retrieved 2020-11-06, from <https://journals.ametsoc.org/jcli/article/30/20/8207/33173/Scale-Dependence-of-Midlatitude-Air-Sea> (Publisher: American Meteorological Society) doi: 10.1175/JCLI-D-17-0159.1
- Bister, M., & Emanuel, K. A. (1998, September). Dissipative heating and hurricane intensity. *Meteorology and Atmospheric Physics*, *65*(3), 233–240. Retrieved 2020-07-01, from <https://doi.org/10.1007/BF01030791> doi: 10.1007/BF01030791
- Blanke, B., & Delecluse, P. (1993, July). Variability of the Tropical Atlantic Ocean Simulated by a General Circulation Model with Two Different Mixed-Layer Physics. *Journal of Physical Oceanography*, *23*(7), 1363–1388. doi: 10.1175/1520-0485(1993)023<1363:VOTTAO>2.0.CO;2
- Browning, S. A., & Goodwin, I. D. (2013, January). Large-Scale Influences on the Evolution of Winter Subtropical Maritime Cyclones Affecting Australia’s East Coast. *Monthly Weather Review*, *141*(7), 2416–2431. doi: 10.1175/MWR-D-12-00312.1
- Bull, C. Y. S., Kiss, A. E., Gupta, A. S., Jourdain, N. C., Argüeso, D., Di Luca, A., & Sérazin, G. (2020). Regional Versus Remote Atmosphere–Ocean Drivers of the Rapid Projected Intensification of the East Australian Current. *Journal of Geophysical Research: Oceans*, *125*(7), e2019JC015889. (eprint: <https://agupubs.onlinelibrary.wiley.com/doi/pdf/10.1029/2019JC015889>) doi: 10.1029/2019JC015889
- Bull, C. Y. S., Kiss, A. E., Jourdain, N. C., England, M. H., & van Sebille, E. (2017). Wind Forced Variability in Eddy Formation, Eddy Shedding, and the Separation of the East Australian Current. *Journal of Geophysical Research: Oceans*, *122*(12), 9980–9998. Retrieved 2020-08-18, from <https://agupubs.onlinelibrary.wiley.com/doi/abs/10.1002/2017JC013311> (eprint:

- <https://agupubs.onlinelibrary.wiley.com/doi/pdf/10.1002/2017JC013311> doi: 10.1002/2017JC013311
- Cavicchia, L., Pepler, A., Dowdy, A., Evans, J., Luca, A. D., & Walsh, K. (2020). Future Changes in the Occurrence of Hybrid Cyclones: The Added Value of Cyclone Classification for the East Australian Low-Pressure Systems. *Geophysical Research Letters*, *47*(6), e2019GL085751. (eprint: <https://agupubs.onlinelibrary.wiley.com/doi/pdf/10.1029/2019GL085751>) doi: 10.1029/2019GL085751
- Cavicchia, L., Pepler, A., Dowdy, A., & Walsh, K. (2019, February). A Physically Based Climatology of the Occurrence and Intensification of Australian East Coast Lows. *Journal of Climate*, *32*(10), 2823–2841. doi: 10.1175/JCLI-D-18-0549.1
- Chambers, C. R. S., Brassington, G. B., Simmonds, I., & Walsh, K. (2014, July). Precipitation changes due to the introduction of eddy-resolved sea surface temperatures into simulations of the “Pasha Bulker” Australian east coast low of June 2007. *Meteorology and Atmospheric Physics*, *125*(1), 1–15. Retrieved 2019-12-18, from <https://doi.org/10.1007/s00703-014-0318-4> doi: 10.1007/s00703-014-0318-4
- Chambers, C. R. S., Brassington, G. B., Walsh, K., & Simmonds, I. (2015, October). Sensitivity of the distribution of thunderstorms to sea surface temperatures in four Australian east coast lows. *Meteorology and Atmospheric Physics*, *127*(5), 499–517. Retrieved 2019-12-18, from <https://doi.org/10.1007/s00703-015-0382-4> doi: 10.1007/s00703-015-0382-4
- Chelton, D. B., & Xie, S.-P. (2010, December). Coupled Ocean-Atmosphere Interaction at Oceanic Mesoscales. *Oceanography*, *23*(4), 52–69. doi: 10.5670/oceanog.2010.05
- Dee, D. P., Uppala, S. M., Simmons, A. J., Berrisford, P., Poli, P., Kobayashi, S., ... Vitart, F. (2011). The ERA-Interim reanalysis: configuration and performance of the data assimilation system. *Quarterly Journal of the Royal Meteorological Society*, *137*(656), 553–597. Retrieved 2020-08-18, from <https://rmets.onlinelibrary.wiley.com/doi/abs/10.1002/qj.828> (eprint: <https://rmets.onlinelibrary.wiley.com/doi/pdf/10.1002/qj.828>) doi: 10.1002/qj.828
- Di Luca, A., Evans, J., Pepler, A., Alexander, L., & Argüeso, D. (2016, June). Evaluating the representation of Australian East Coast Lows in a regional climate model ensemble. *Journal of Southern Hemisphere Earth System Science*, *66*, 108–124. doi: 10.22499/3.6602.003
- Di Luca, A., Evans, J. P., Pepler, A., Alexander, L., & Argüeso, D. (2015, November). Resolution Sensitivity of Cyclone Climatology over Eastern Australia Using Six Reanalysis Products. *Journal of Climate*, *28*(24), 9530–9549. doi: 10.1175/JCLI-D-14-00645.1
- Donlon, C. J., Martin, M., Stark, J., Roberts-Jones, J., Fiedler, E., & Wimmer, W. (2012, January). The Operational Sea Surface Temperature and Sea Ice Analysis (OSTIA) system. *Remote Sensing of Environment*, *116*, 140–158. Retrieved 2020-09-09, from <http://www.sciencedirect.com/science/article/pii/S0034425711002197> doi: 10.1016/j.rse.2010.10.017
- Dowdy, A. J., Mills, G. A., & Timbal, B. (2013). Large-scale diagnostics of extratropical cyclogenesis in eastern Australia. *International Journal of Climatology*, *33*(10), 2318–2327. Retrieved 2020-11-06, from <https://rmets.onlinelibrary.wiley.com/doi/abs/10.1002/joc.3599> (eprint: <https://rmets.onlinelibrary.wiley.com/doi/pdf/10.1002/joc.3599>) doi: 10.1002/joc.3599
- Dowdy, A. J., Mills, G. A., Timbal, B., & Wang, Y. (2012, August). Changes in the Risk of Extratropical Cyclones in Eastern Australia. *Journal of Climate*, *26*(4), 1403–1417. doi: 10.1175/JCLI-D-12-00192.1

- Dowdy, A. J., Mills, G. A., Timbal, B., & Wang, Y. (2014, April). Fewer large waves projected for eastern Australia due to decreasing storminess. *Nature Climate Change*, *4*(4), 283–286. doi: 10.1038/nclimate2142
- Dowdy, A. J., Pepler, A., Di Luca, A., Cavicchia, L., Mills, G., Evans, J. P., . . . Walsh, K. (2019, October). Review of Australian east coast low pressure systems and associated extremes. *Climate Dynamics*, *53*(7), 4887–4910. Retrieved 2019-12-10, from <https://doi.org/10.1007/s00382-019-04836-8> doi: 10.1007/s00382-019-04836-8
- Drosowsky, W. (2005). The latitude of the subtropical ridge over Eastern Australia: The L index revisited. *International Journal of Climatology*, *25*(10), 1291–1299. doi: 10.1002/joc.1196
- Dudhia, J. (1989, October). Numerical Study of Convection Observed during the Winter Monsoon Experiment Using a Mesoscale Two-Dimensional Model. *Journal of the Atmospheric Sciences*, *46*(20), 3077–3107. Retrieved 2021-04-19, from https://journals.ametsoc.org/view/journals/atsc/46/20/1520-0469_1989_046_3077_nsocod_2_0_co_2.xml (Publisher: American Meteorological Society Section: Journal of the Atmospheric Sciences) doi: 10.1175/1520-0469(1989)046<3077:NSOCOD>2.0.CO;2
- Dutheil, C., Lengaigne, M., Bador, M., Vialard, J., Lefèvre, J., Jourdain, N. C., . . . Menkès, C. (2020, March). Impact of projected sea surface temperature biases on tropical cyclones projections in the South Pacific. *Scientific Reports*, *10*(1), 4838. Retrieved 2020-11-24, from <https://www.nature.com/articles/s41598-020-61570-6> (Number: 1 Publisher: Nature Publishing Group) doi: 10.1038/s41598-020-61570-6
- Emanuel, K. A. (1999, October). Thermodynamic control of hurricane intensity. *Nature*, *401*(6754), 665–669. Retrieved 2020-06-11, from <https://www.nature.com/articles/44326> (Number: 6754 Publisher: Nature Publishing Group) doi: 10.1038/44326
- Evans, J. P., Ji, F., Lee, C., Smith, P., Argüeso, D., & Fita, L. (2014, April). Design of a regional climate modelling projection ensemble experiment – NAR-CliM. *Geoscientific Model Development*, *7*(2), 621–629. Retrieved 2021-03-03, from <https://gmd.copernicus.org/articles/7/621/2014/> (Publisher: Copernicus GmbH) doi: <https://doi.org/10.5194/gmd-7-621-2014>
- Frenger, I., Gruber, N., Knutti, R., & Münnich, M. (2013, August). Imprint of Southern Ocean eddies on winds, clouds and rainfall. *Nature Geoscience*, *6*(8), 608–612. Retrieved 2015-11-22, from <http://www.nature.com/biblioplanets.gate.inist.fr/ngeo/journal/v6/n8/full/ngeo1863.html> doi: 10.1038/ngeo1863
- Hart, R. E. (2003, April). A Cyclone Phase Space Derived from Thermal Wind and Thermal Asymmetry. *Monthly Weather Review*, *131*(4), 585–616. doi: 10.1175/1520-0493(2003)131(0585:ACPSDF)2.0.CO;2
- Hersbach, H., Bell, B., Berrisford, P., Hirahara, S., Horányi, A., Muñoz-Sabater, J., . . . Thépaut, J.-N. (2020). The ERA5 global reanalysis. *Quarterly Journal of the Royal Meteorological Society*, *146*(730), 1999–2049. Retrieved 2020-09-01, from <https://rmets.onlinelibrary.wiley.com/doi/abs/10.1002/qj.3803> (_eprint: <https://rmets.onlinelibrary.wiley.com/doi/pdf/10.1002/qj.3803>) doi: 10.1002/qj.3803
- Hewitt, H. T., Bell, M. J., Chassignet, E. P., Czaja, A., Ferreira, D., Griffies, S. M., . . . Roberts, M. J. (2017, December). Will high-resolution global ocean models benefit coupled predictions on short-range to climate timescales? *Ocean Modelling*, *120*, 120–136. Retrieved 2018-11-15, from <http://www.sciencedirect.com/science/article/pii/S1463500317301774> doi: 10.1016/j.ocemod.2017.11.002
- Hong, S.-Y., Dudhia, J., & Chen, S.-H. (2004, January). A Revised Approach to Ice Microphysical Processes for the Bulk Parameterization of Clouds

- and Precipitation. *Monthly Weather Review*, 132(1), 103–120. Retrieved 2021-04-19, from https://journals.ametsoc.org/view/journals/mwre/132/1/1520-0493.2004.132_0103_aratim_2.0.co_2.xml (Publisher: American Meteorological Society Section: Monthly Weather Review) doi: 10.1175/1520-0493(2004)132<0103:ARATIM>2.0.CO;2
- Janjić, Z. I. (1994, May). The Step-Mountain Eta Coordinate Model: Further Developments of the Convection, Viscous Sublayer, and Turbulence Closure Schemes. *Monthly Weather Review*, 122(5), 927–945. Retrieved 2021-04-19, from https://journals.ametsoc.org/view/journals/mwre/122/5/1520-0493.1994.122_0927_tsmecm_2.0.co_2.xml (Publisher: American Meteorological Society Section: Monthly Weather Review) doi: 10.1175/1520-0493(1994)122<0927:TSMECM>2.0.CO;2
- Jourdain, N. C., Lengaigne, M., Vialard, J., Madec, G., Menkes, C. E., Vincent, E. M., ... Barnier, B. (2013, January). Observation-Based Estimates of Surface Cooling Inhibition by Heavy Rainfall under Tropical Cyclones. *Journal of Physical Oceanography*, 43(1), 205–221. (Publisher: American Meteorological Society) doi: 10.1175/JPO-D-12-085.1
- Jullien, S., Marchesiello, P., Menkes, C. E., Lefèvre, J., Jourdain, N. C., Samson, G., & Lengaigne, M. (2014, November). Ocean feedback to tropical cyclones: climatology and processes. *Climate Dynamics*, 43(9), 2831–2854. doi: 10.1007/s00382-014-2096-6
- Jullien, S., Masson, S., Oerder, V., Samson, G., Colas, F., & Renault, L. (2020, April). Impact of Ocean–Atmosphere Current Feedback on Ocean Mesoscale Activity: Regional Variations and Sensitivity to Model Resolution. *Journal of Climate*, 33(7), 2585–2602. Retrieved 2020-10-20, from <https://journals.ametsoc.org/jcli/article/33/7/2585/346415/Impact-of-Ocean-Atmosphere-Current-Feedback-on> (Publisher: American Meteorological Society) doi: 10.1175/JCLI-D-19-0484.1
- Jullien, S., Menkes, C. E., Marchesiello, P., Jourdain, N. C., Lengaigne, M., Koch-Larrouy, A., ... Faure, V. (2012, November). Impact of Tropical Cyclones on the Heat Budget of the South Pacific Ocean. *Journal of Physical Oceanography*, 42(11), 1882–1906. (Publisher: American Meteorological Society) doi: 10.1175/JPO-D-11-0133.1
- Kanamitsu, M., Ebisuzaki, W., Woollen, J., Yang, S.-K., Hnilo, J. J., Fiorino, M., & Potter, G. L. (2002, November). NCEP–DOE AMIP-II Reanalysis (R-2). *Bulletin of the American Meteorological Society*, 83(11), 1631–1644. Retrieved 2021-04-29, from <https://journals.ametsoc.org/view/journals/bams/83/11/bams-83-11-1631.xml> (Publisher: American Meteorological Society Section: Bulletin of the American Meteorological Society) doi: 10.1175/BAMS-83-11-1631
- Klaver, R., Haarsma, R., Vidale, P. L., & Hazeleger, W. (2020). Effective resolution in high resolution global atmospheric models for climate studies. *Atmospheric Science Letters*, 21(4), e952. Retrieved 2021-04-29, from <https://rmets.onlinelibrary.wiley.com/doi/abs/10.1002/asl.952> (_eprint: <https://rmets.onlinelibrary.wiley.com/doi/pdf/10.1002/asl.952>) doi: <https://doi.org/10.1002/asl.952>
- Lemarié, F. (2015, August). *Numerical modification of atmospheric models to include the feedback of oceanic currents on air-sea fluxes in ocean-atmosphere coupled models* (report). INRIA Grenoble - Rhône-Alpes ; Laboratoire Jean Kuntzmann ; Université de Grenoble I - Joseph Fourier ; INRIA. Retrieved 2021-03-08, from <https://hal.inria.fr/hal-01184711>
- Lengaigne, M., Neetu, S., Samson, G., Vialard, J., Krishnamohan, K. S., Masson, S., ... Menkes, C. E. (2019, January). Influence of air–sea coupling on Indian Ocean tropical cyclones. *Climate Dynamics*, 52(1), 577–598. doi: 10.1007/s00382-018-4152-0

- Le Sommer, J., Penduff, T., Theetten, S., Madec, G., & Barnier, B. (2009, January). How momentum advection schemes influence current-topography interactions at eddy permitting resolution. *Ocean Modelling*, *29*(1), 1–14. doi: 10.1016/j.ocemod.2008.11.007
- Lim, E.-P., & Simmonds, I. (2002, September). Explosive Cyclone Development in the Southern Hemisphere and a Comparison with Northern Hemisphere Events. *Monthly Weather Review*, *130*(9), 2188–2209. Retrieved 2020-11-06, from <https://journals.ametsoc.org/mwr/article/130/9/2188/66764/Explosive-Cyclone-Development-in-the-Southern> (Publisher: American Meteorological Society) doi: 10.1175/1520-0493(2002)130<2188:ECDITS>2.0.CO;2
- Ma, X., Chang, P., Saravanan, R., Montuoro, R., Nakamura, H., Wu, D., ... Wu, L. (2016, November). Importance of Resolving Kuroshio Front and Eddy Influence in Simulating the North Pacific Storm Track. *Journal of Climate*, *30*(5), 1861–1880. doi: 10.1175/JCLI-D-16-0154.1
- Ma, X., Jing, Z., Chang, P., Liu, X., Montuoro, R., Small, R. J., ... Wu, L. (2016, July). Western boundary currents regulated by interaction between ocean eddies and the atmosphere. *Nature*, *535*(7613), 533–537. Retrieved 2018-09-21, from <https://www.nature.com/articles/nature18640> doi: 10.1038/nature18640
- Madec, G. (2008). *NEMO ocean engine* (Note du Pole de modélisation No. 27). France: Institut Pierre-Simon Laplace (IPSL).
- McInnes, K. L., Leslie, L. M., & McBride, J. L. (1992). Numerical simulation of cut-off lows on the Australian east coast: Sensitivity to sea-surface temperature. *International Journal of Climatology*, *12*(8), 783–795. doi: 10.1002/joc.3370120803
- Mlawer, E. J., Taubman, S. J., Brown, P. D., Iacono, M. J., & Clough, S. A. (1997). Radiative transfer for inhomogeneous atmospheres: RRTM, a validated correlated-k model for the longwave. *Journal of Geophysical Research: Atmospheres*, *102*(D14), 16663–16682. Retrieved 2021-04-19, from <https://agupubs.onlinelibrary.wiley.com/doi/abs/10.1029/97JD00237> (eprint: <https://agupubs.onlinelibrary.wiley.com/doi/pdf/10.1029/97JD00237>) doi: <https://doi.org/10.1029/97JD00237>
- Oerder, V., Colas, F., Echevin, V., Masson, S., Hourdin, C., Jullien, S., ... Lemarié, F. (2016, October). Mesoscale SST–wind stress coupling in the Peru–Chile current system: Which mechanisms drive its seasonal variability? *Climate Dynamics*, *47*(7), 2309–2330. Retrieved 2020-08-18, from <https://doi.org/10.1007/s00382-015-2965-7> doi: 10.1007/s00382-015-2965-7
- Oke, P. R., Roughan, M., Cetina-Heredia, P., Pilo, G. S., Ridgway, K. R., Rykova, T., ... Vitarelli, E. (2019, September). Revisiting the circulation of the East Australian Current: Its path, separation, and eddy field. *Progress in Oceanography*, *176*, 102139. Retrieved 2020-10-27, from <http://www.sciencedirect.com/science/article/pii/S0079661118301745> doi: 10.1016/j.pocean.2019.102139
- Penduff, T., Le Sommer, J., Barnier, B., Treguier, A.-M., Molines, J., & Madec, G. (2007, December). Influence of numerical schemes on current-topography interactions in 1/4 degrees global ocean simulations. *Ocean Science*, *3*(4), 509–524.
- Pepler, A., & Coutts-Smith, A. (2013, December). A new, objective, database of East Coast Lows. *Australian Meteorological and Oceanographic Journal*, *63*, 461–472. doi: 10.22499/2.6304.001
- Pepler, A. S., Alexander, L. V., Evans, J. P., & Sherwood, S. C. (2016). The influence of local sea surface temperatures on Australian east coast cyclones. *Journal of Geophysical Research: Atmospheres*, *121*(22), 13,352–13,363. Retrieved 2019-12-18, from <https://agupubs.onlinelibrary.wiley.com/doi/>

- abs/10.1002/2016JD025495 doi: 10.1002/2016JD025495
- Pepler, A. S., Coutts-Smith, A., & Timbal, B. (2014). The role of East Coast Lows on rainfall patterns and inter-annual variability across the East Coast of Australia. *International Journal of Climatology*, *34*(4), 1011–1021. Retrieved 2020-08-18, from <https://rmets.onlinelibrary.wiley.com/doi/abs/10.1002/joc.3741> (_eprint: <https://rmets.onlinelibrary.wiley.com/doi/pdf/10.1002/joc.3741>) doi: 10.1002/joc.3741
- Pepler, A. S., Di Luca, A., Ji, F., Alexander, L. V., Evans, J. P., & Sherwood, S. C. (2014, October). Impact of Identification Method on the Inferred Characteristics and Variability of Australian East Coast Lows. *Monthly Weather Review*, *143*(3), 864–877. Retrieved 2019-12-04, from <https://journals.ametsoc.org/doi/abs/10.1175/MWR-D-14-00188.1> doi: 10.1175/MWR-D-14-00188.1
- Pepler, A. S., Di Luca, A., Ji, F., Alexander, L. V., Evans, J. P., & Sherwood, S. C. (2016). Projected changes in east Australian midlatitude cyclones during the 21st century. *Geophysical Research Letters*, *43*(1), 334–340. doi: 10.1002/2015GL067267
- Piazza, M., Terray, L., Boé, J., Maisonnave, E., & Sanchez-Gomez, E. (2016, March). Influence of small-scale North Atlantic sea surface temperature patterns on the marine boundary layer and free troposphere: a study using the atmospheric ARPEGE model. *Climate Dynamics*, *46*(5), 1699–1717. Retrieved 2019-12-04, from <https://doi.org/10.1007/s00382-015-2669-z> doi: 10.1007/s00382-015-2669-z
- Quinting, J. F., Catto, J. L., & Reeder, M. J. (2019). Synoptic climatology of hybrid cyclones in the Australian region. *Quarterly Journal of the Royal Meteorological Society*, *145*(718), 288–302. Retrieved 2020-07-03, from <https://rmets.onlinelibrary.wiley.com/doi/abs/10.1002/qj.3431> (_eprint: <https://rmets.onlinelibrary.wiley.com/doi/pdf/10.1002/qj.3431>) doi: 10.1002/qj.3431
- Rayner, N. A., Parker, D. E., Horton, E. B., Folland, C. K., Alexander, L. V., Rowell, D. P., ... Kaplan, A. (2003). Global analyses of sea surface temperature, sea ice, and night marine air temperature since the late nineteenth century. *Journal of Geophysical Research: Atmospheres*, *108*(D14). Retrieved 2020-09-09, from <https://agupubs.onlinelibrary.wiley.com/doi/abs/10.1029/2002JD002670> (_eprint: <https://agupubs.onlinelibrary.wiley.com/doi/pdf/10.1029/2002JD002670>) doi: 10.1029/2002JD002670
- Renault, L., Masson, S., Arsouze, T., Madec, G., & McWilliams, J. C. (2020). Recipes for How to Force Oceanic Model Dynamics. *Journal of Advances in Modeling Earth Systems*, *12*(2), e2019MS001715. Retrieved 2021-03-01, from <https://agupubs.onlinelibrary.wiley.com/doi/abs/10.1029/2019MS001715> (_eprint: <https://agupubs.onlinelibrary.wiley.com/doi/pdf/10.1029/2019MS001715>) doi: <https://doi.org/10.1029/2019MS001715>
- Renault, L., Masson, S., Oerder, V., Jullien, S., & Colas, F. (2019). Disentangling the Mesoscale Ocean-Atmosphere Interactions. *Journal of Geophysical Research: Oceans*, *124*(3), 2164–2178. doi: 10.1029/2018JC014628
- Renault, L., McWilliams, J. C., & Penven, P. (2017, June). Modulation of the Agulhas Current Retroreflection and Leakage by Oceanic Current Interaction with the Atmosphere in Coupled Simulations. *Journal of Physical Oceanography*, *47*(8), 2077–2100. Retrieved 2018-09-12, from <https://journals.ametsoc.org/doi/10.1175/JPO-D-16-0168.1> doi: 10.1175/JPO-D-16-0168.1
- Renault, L., Molemaker, M. J., Gula, J., Masson, S., & McWilliams, J. C. (2016,

- September). Control and Stabilization of the Gulf Stream by Oceanic Current Interaction with the Atmosphere. *Journal of Physical Oceanography*, 46(11), 3439–3453. Retrieved 2018-09-19, from <https://journals.ametsoc.org/doi/10.1175/JPO-D-16-0115.1> doi: 10.1175/JPO-D-16-0115.1
- Renault, L., Molemaker, M. J., McWilliams, J. C., Shchepetkin, A. F., Lemarié, F., Chelton, D., ... Hall, A. (2016, March). Modulation of Wind Work by Oceanic Current Interaction with the Atmosphere. *Journal of Physical Oceanography*, 46(6), 1685–1704. Retrieved 2018-09-19, from <https://journals.ametsoc.org/doi/10.1175/JPO-D-15-0232.1> doi: 10.1175/JPO-D-15-0232.1
- Rienecker, M. M., Suarez, M. J., Gelaro, R., Todling, R., Bacmeister, J., Liu, E., ... Woollen, J. (2011, July). MERRA: NASA’s Modern-Era Retrospective Analysis for Research and Applications. *Journal of Climate*, 24(14), 3624–3648. Retrieved 2021-04-29, from <https://journals.ametsoc.org/view/journals/clim/24/14/jcli-d-11-00015.1.xml> (Publisher: American Meteorological Society Section: Journal of Climate) doi: 10.1175/JCLI-D-11-00015.1
- Roberts, M. J., Camp, J., Seddon, J., Vidale, P. L., Hodges, K., Vanniere, B., ... Ullrich, P. (2020, April). Impact of Model Resolution on Tropical Cyclone Simulation Using the HighResMIP–PRIMAVERA Multimodel Ensemble. *Journal of Climate*, 33(7), 2557–2583. Retrieved 2021-04-29, from <https://journals.ametsoc.org/view/journals/clim/33/7/jcli-d-19-0639.1.xml> (Publisher: American Meteorological Society Section: Journal of Climate) doi: 10.1175/JCLI-D-19-0639.1
- Saha, S., Moorthi, S., Pan, H.-L., Wu, X., Wang, J., Nadiga, S., ... Goldberg, M. (2010, August). The NCEP Climate Forecast System Reanalysis. *Bulletin of the American Meteorological Society*, 91(8), 1015–1058. Retrieved 2021-04-29, from <https://journals.ametsoc.org/view/journals/bams/91/8/2010bams3001.1.xml> (Publisher: American Meteorological Society Section: Bulletin of the American Meteorological Society) doi: 10.1175/2010BAMS3001.1
- Samson, G., Masson, S., Lengaigne, M., Keerthi, M. G., Vialard, J., Pous, S., ... Marchesiello, P. (2014). The NOW regional coupled model: Application to the tropical Indian Ocean climate and tropical cyclone activity. *Journal of Advances in Modeling Earth Systems*, 6(3), 700–722. Retrieved 2019-11-15, from <https://agupubs.onlinelibrary.wiley.com/doi/abs/10.1002/2014MS000324> doi: 10.1002/2014MS000324
- Short, A. D., & Trenaman, N. L. (1992). Wave climate of the Sydney region, an energetic and highly variable ocean wave regime. *Marine and Freshwater Research*, 43(4), 765–791. doi: 10.1071/mf9920765
- Skamarock, W. C., Klemp, J. B., Dudhia, J., Gill, D. O., Barker, D. M., Wang, W., & Powers, J. G. (2008). *A description of the Advanced Research WRF version 3*.
- Small, R. J., Bryan, F. O., Bishop, S. P., Larson, S., & Tomas, R. A. (2020, January). What Drives Upper-Ocean Temperature Variability in Coupled Climate Models and Observations? *Journal of Climate*, 33(2), 577–596. Retrieved 2020-11-06, from <https://journals.ametsoc.org/jcli/article/33/2/577/346234/What-Drives-Upper-Ocean-Temperature-Variability-in> (Publisher: American Meteorological Society) doi: 10.1175/JCLI-D-19-0295.1
- Small, R. J., deSzoeko, S. P., Xie, S. P., O’Neill, L., Seo, H., Song, Q., ... Minobe, S. (2008, August). Air–sea interaction over ocean fronts and eddies. *Dynamics of Atmospheres and Oceans*, 45(3), 274–319. doi: 10.1016/j.dynatmoce.2008.01.001
- Smirnov, D., Newman, M., Alexander, M. A., Kwon, Y.-O., & Frankignoul, C. (2014, November). Investigating the Local Atmospheric Response to a Realistic Shift in the Oyashio Sea Surface Temperature Front. *Journal of Climate*,

- 28(3), 1126–1147. doi: 10.1175/JCLI-D-14-00285.1
- Sérazin, G., Penduff, T., Grégorio, S., Barnier, B., Molines, J.-M., & Terray, L. (2014, December). Intrinsic Variability of Sea Level from Global Ocean Simulations: Spatiotemporal Scales. *Journal of Climate*, 28(10), 4279–4292. doi: 10.1175/JCLI-D-14-00554.1
- Tippett, M. K., Camargo, S. J., & Sobel, A. H. (2010, December). A Poisson Regression Index for Tropical Cyclone Genesis and the Role of Large-Scale Vorticity in Genesis. *Journal of Climate*, 24(9), 2335–2357. Retrieved 2020-05-13, from <https://journals.ametsoc.org/doi/10.1175/2010JCLI3811.1> (Publisher: American Meteorological Society) doi: 10.1175/2010JCLI3811.1
- Valcke, S. (2013, March). The OASIS3 coupler: a European climate modelling community software. *Geoscientific Model Development*, 6(2), 373–388. (Publisher: Copernicus GmbH) doi: <https://doi.org/10.5194/gmd-6-373-2013>
- Vincent, E. M., Lengaigne, M., Madec, G., Vialard, J., Samson, G., Jourdain, N. C., ... Jullien, S. (2012). Processes setting the characteristics of sea surface cooling induced by tropical cyclones. *Journal of Geophysical Research: Oceans*, 117(C2). (eprint: <https://agupubs.onlinelibrary.wiley.com/doi/pdf/10.1029/2011JC007396>) doi: 10.1029/2011JC007396
- Willison, J., Robinson, W. A., & Lackmann, G. M. (2013, January). The Importance of Resolving Mesoscale Latent Heating in the North Atlantic Storm Track. *Journal of the Atmospheric Sciences*, 70(7), 2234–2250. Retrieved 2019-12-05, from <https://journals.ametsoc.org/doi/full/10.1175/JAS-D-12-0226.1> doi: 10.1175/JAS-D-12-0226.1
- Xie, S.-P. (2004, February). Satellite Observations of Cool Ocean–Atmosphere Interaction. *Bulletin of the American Meteorological Society*, 85(2), 195–208. Retrieved 2018-11-15, from <https://journals.ametsoc.org/doi/10.1175/BAMS-85-2-195> doi: 10.1175/BAMS-85-2-195
- Zhang, X., Ma, X., & Wu, L. (2019). Effect of Mesoscale Oceanic Eddies on Extratropical Cyclogenesis: A Tracking Approach. *Journal of Geophysical Research: Atmospheres*, 124(12), 6411–6422. Retrieved 2019-12-05, from <https://agupubs.onlinelibrary.wiley.com/doi/abs/10.1029/2019JD030595> doi: 10.1029/2019JD030595

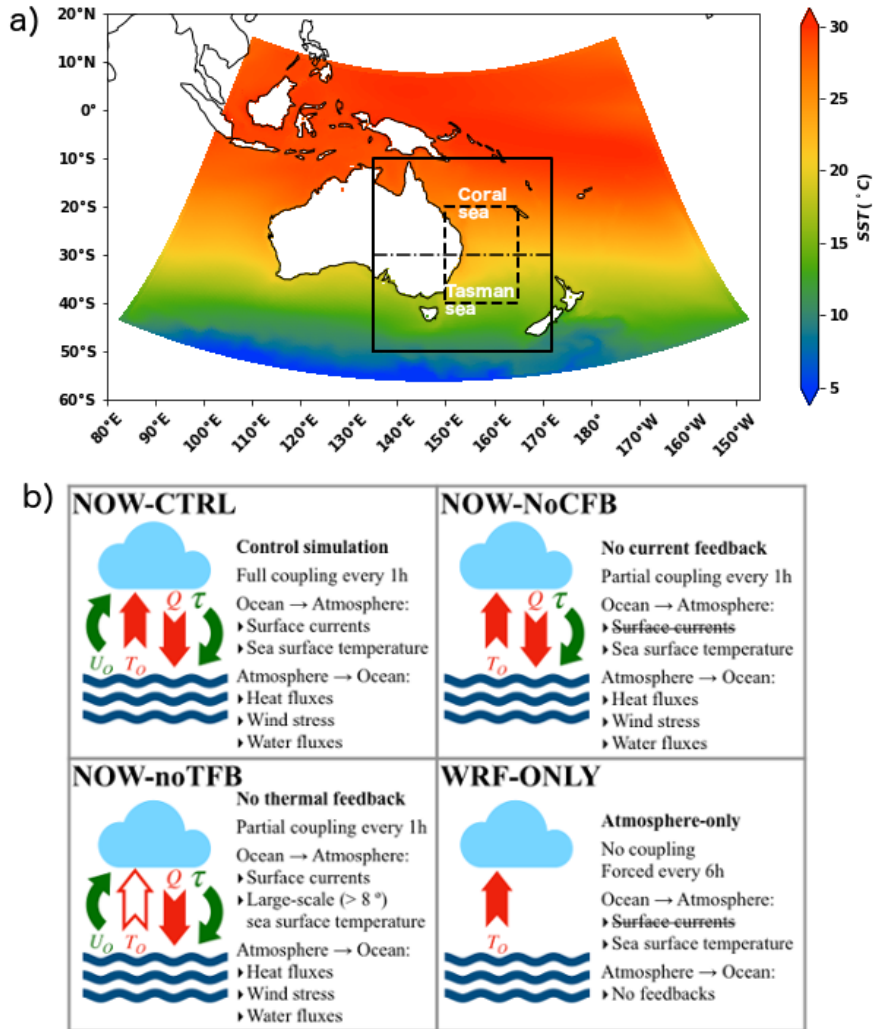


Figure 1. a) Mean SST of the NOW-CTRL experiment simulated over the CORDEX Australasian domain. The region where low-pressure systems are tracked is drawn with black plain lines, while the analysis region where ECL are defined is shown with dashed lines. The dashed-dotted line represent the 30°S cutoff. b) Summary of the air-sea coupling for the different experiments.

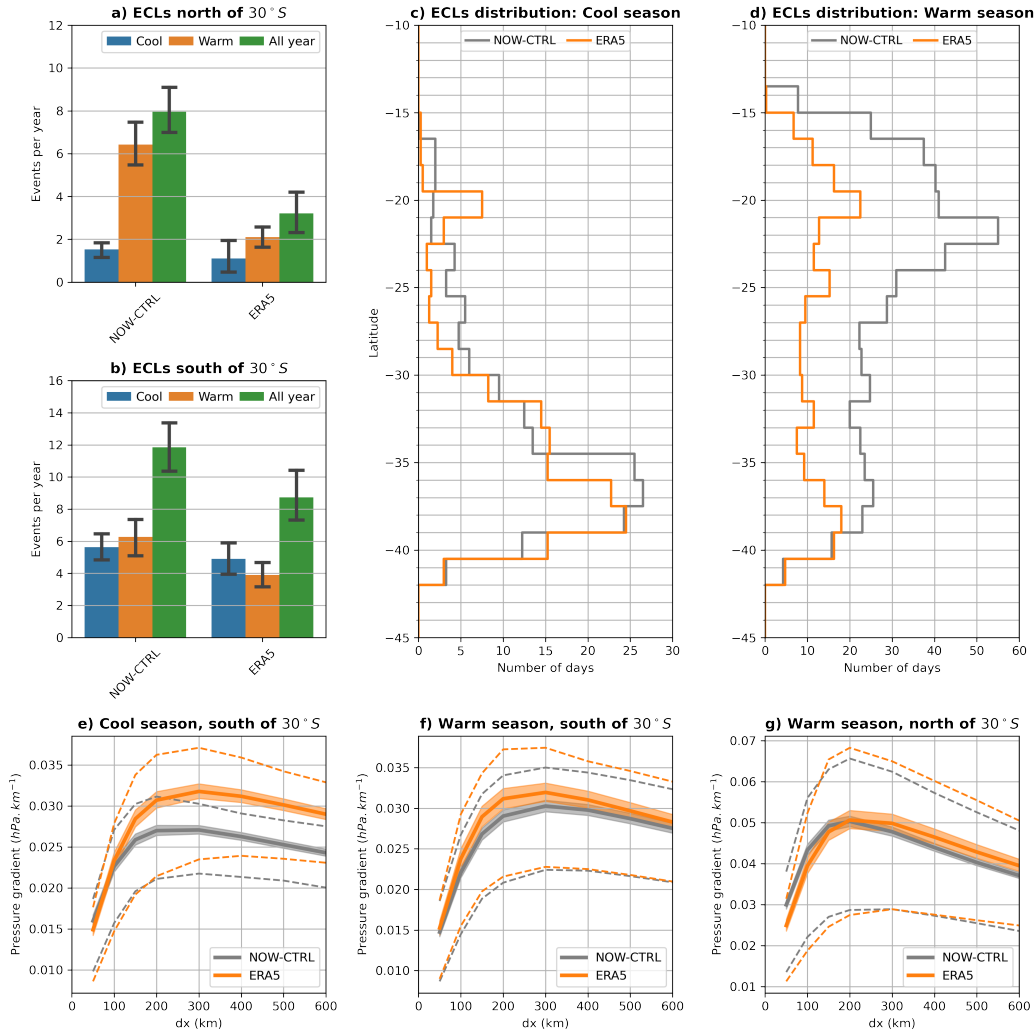


Figure 2. Average number of East Coast Low (ECL) events per year in the NOW-CTRL simulation and in the ERA5 dataset separated into a warm season (November-April) and a cool season (May-October) for: a) northern ECLs (NECLs, $< 30^{\circ}S$), b) southern ECLs (SECLs, $> 30^{\circ}S$). The error bar represent the uncertainty due to interannual variability, estimated using a bootstrap method on 1000 realisations with a confidence interval of 90%. c) Meridional distribution of the number of ECL days during the cool season and during the warm season (panel d). e-g) Isotropic distribution of the pressure gradient across the cyclone; the plain curves represent the mean pressure gradient, the dashed curves correspond to the 25% and 75% percentiles and confidence intervals at 5% and 95% are drawn using coloured shading and estimated from bootstrapping.

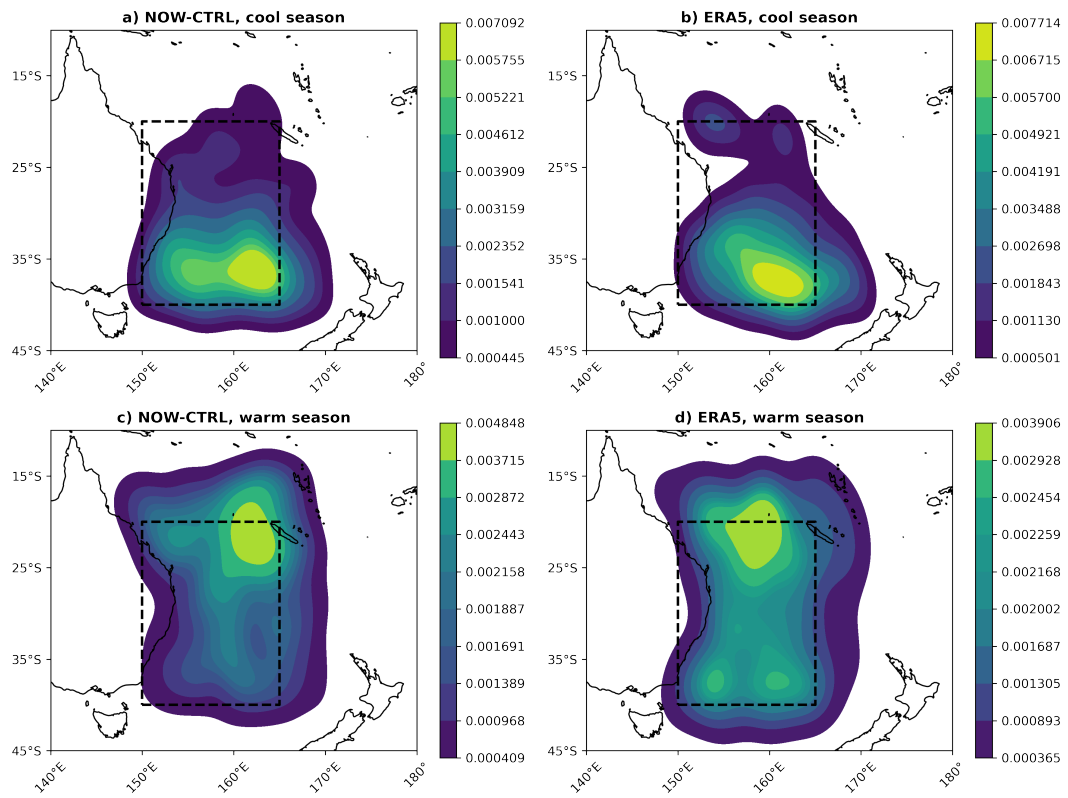


Figure 3. Probability density function of ECL events for NOW-CTRL and ERA5 during cool and warm seasons with the ECL region plotted with dashed lines.

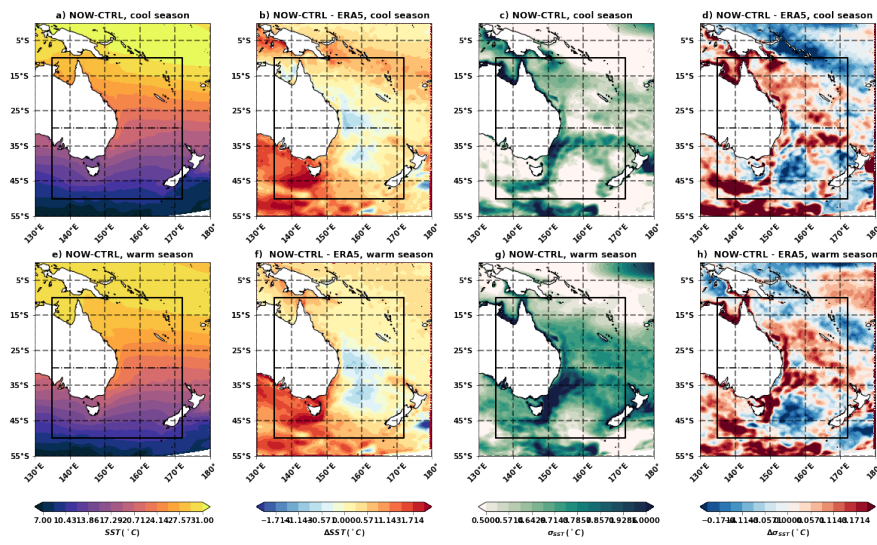


Figure 4. Sea surface temperature climatology from NOW-CTRL (a, e) and associated difference with ERA5 (b, f). Sea surface temperature variability from NOW-CTRL (c, g) and associated difference with ERA5 (d, h), estimated using the daily standard deviation of daily timeseries deprived of the seasonal cycle.

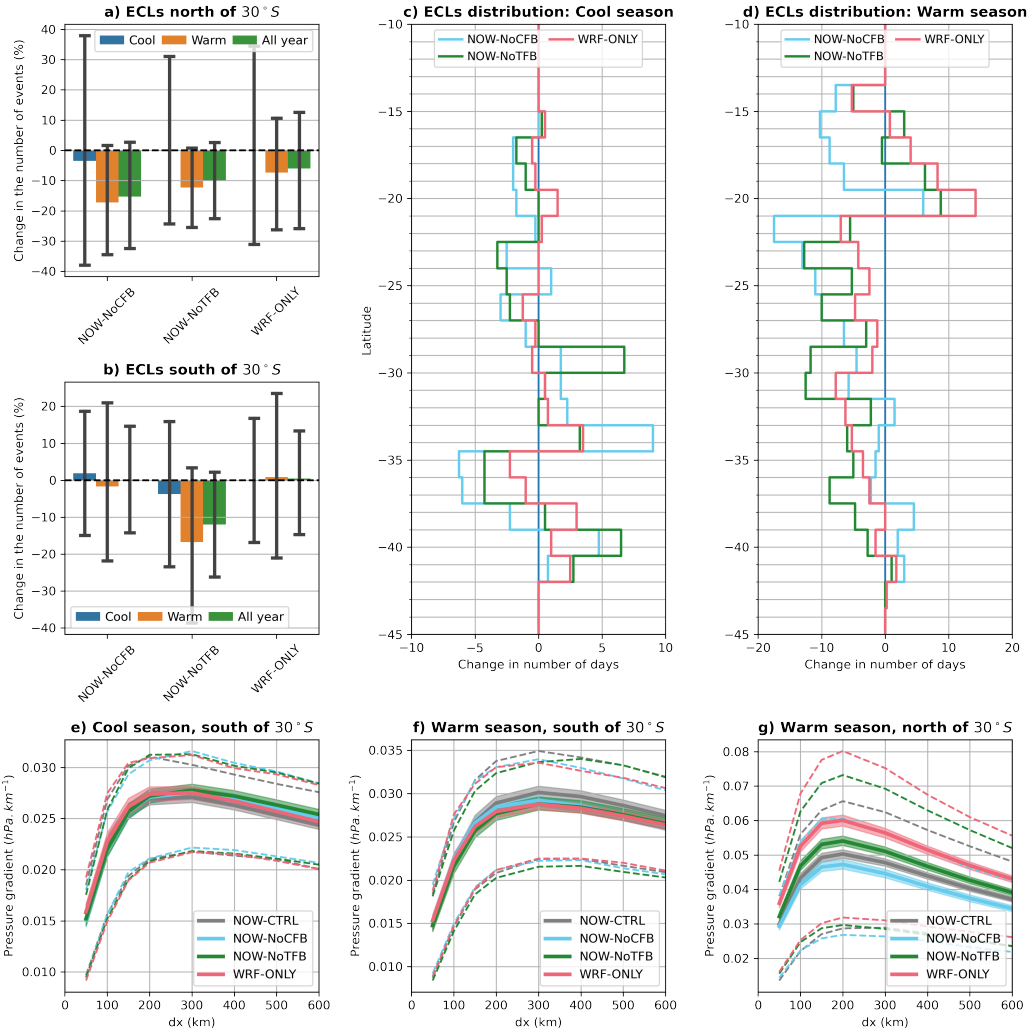


Figure 5. Same as Figure 2 but for the changes relative to NOW-CTRL for the three sensitivity experiments NOW-NoCFB, NOW-NoTFB and WRF-ONLY. In a-b), the bootstrap method is applied on yearly difference between experiments.

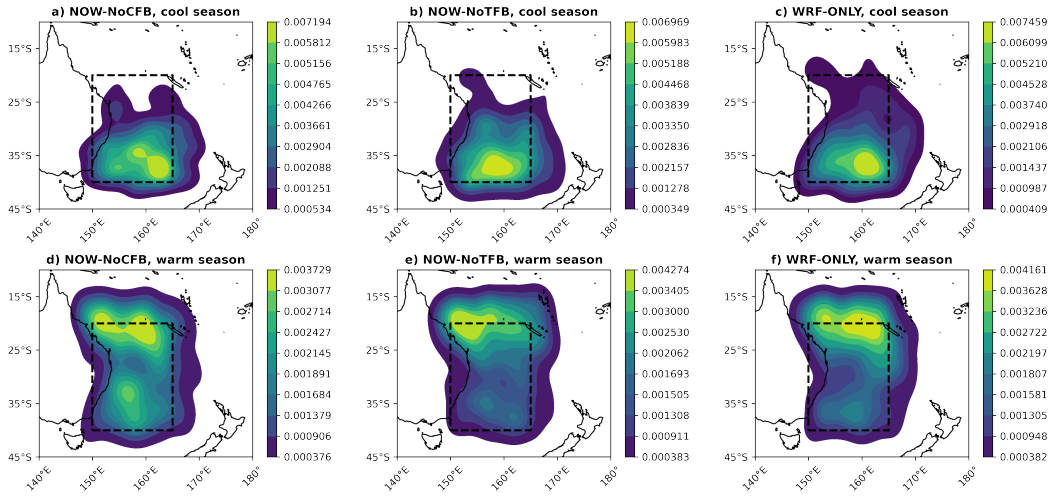


Figure 6. Same as Figure 3 but for the three sensitivity experiments NOW-NoCFB, NOW-NoTFB and WRF-ONLY

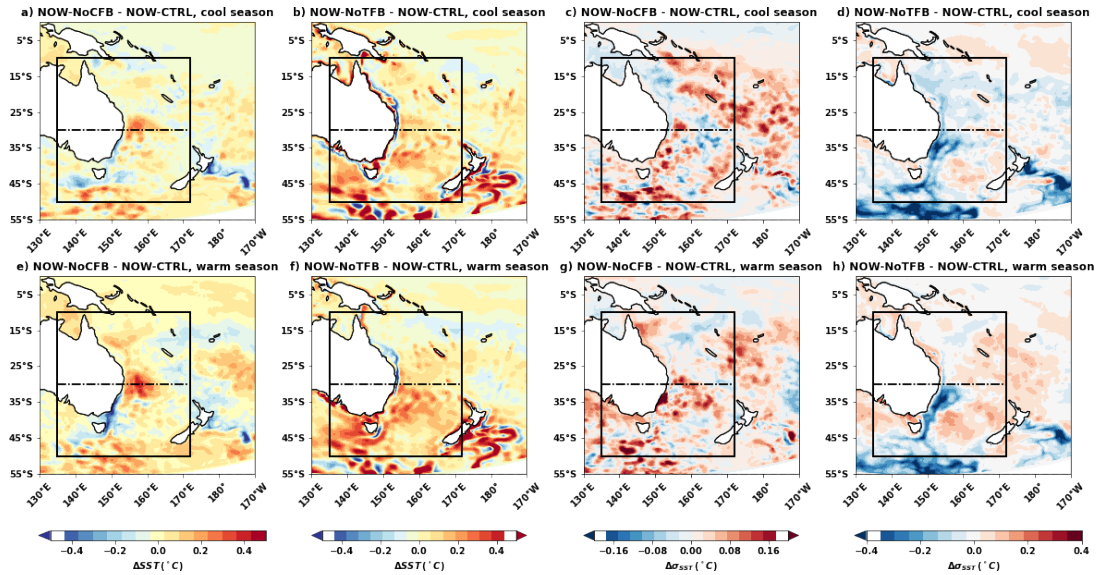


Figure 7. (a, b, e, f) Same as Figure 4b,f but for the changes in the mean SST relative to NOW-CTRL for the two sensitivity experiments NOW-NoCFB, NOW-NoTFB. (c, d, g, h) Same as Figure 4d,h for the changes in SST variability.

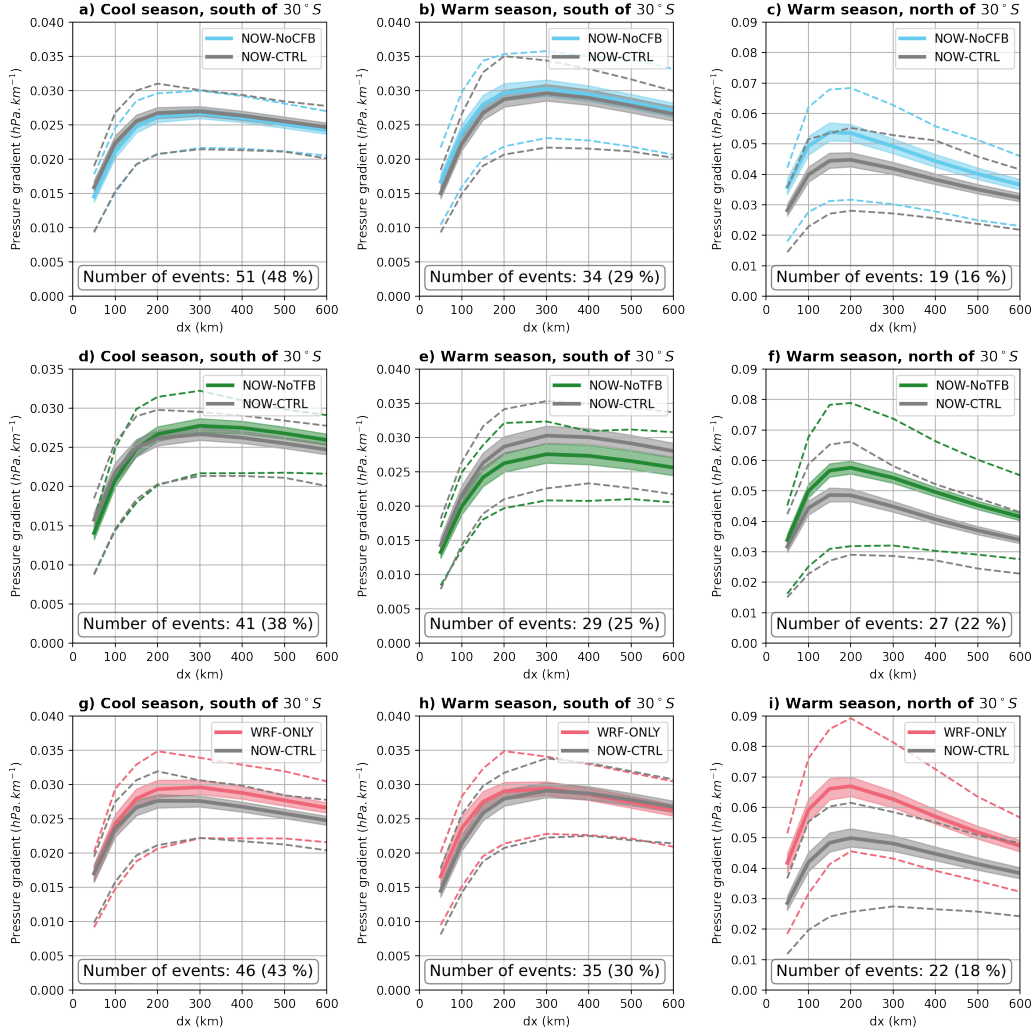


Figure 8. Radial profile of the pressure gradient across the cyclone for common events between: a-c) NOW-CTRL and NOW-NoCFB, d-f) NOW-CTRL and NOW-NoTFB, g-i) NOW-CTRL and WRF-NOW. Events are classified into three temporal and spatial categories: a,d,g) cool season south of $30^{\circ}S$, b,e,h) warm season south of $30^{\circ}S$, c,f,i) warm season north of $30^{\circ}S$. The number of common events is shown for each case along with the proportion of events in NOW-CTRL. Confidence intervals at 5% and 95% are drawn using coloured shading and estimated from bootstrapping.

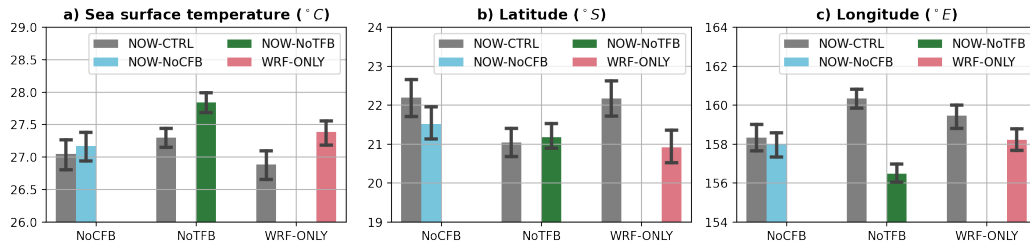


Figure 9. Pre-storm ambient SST (a) averaged between 10 and 5 days prior to NECL passing (north of $30^{\circ}S$) during the warm season and within a 200 km radius. Storm latitude (b) and longitude (c) during the warm season. Only common NECL events are shown, which is why there are three different values for NOW-CTRL. Confidence intervals at 5% and 95% are evaluated using a bootstrap method.

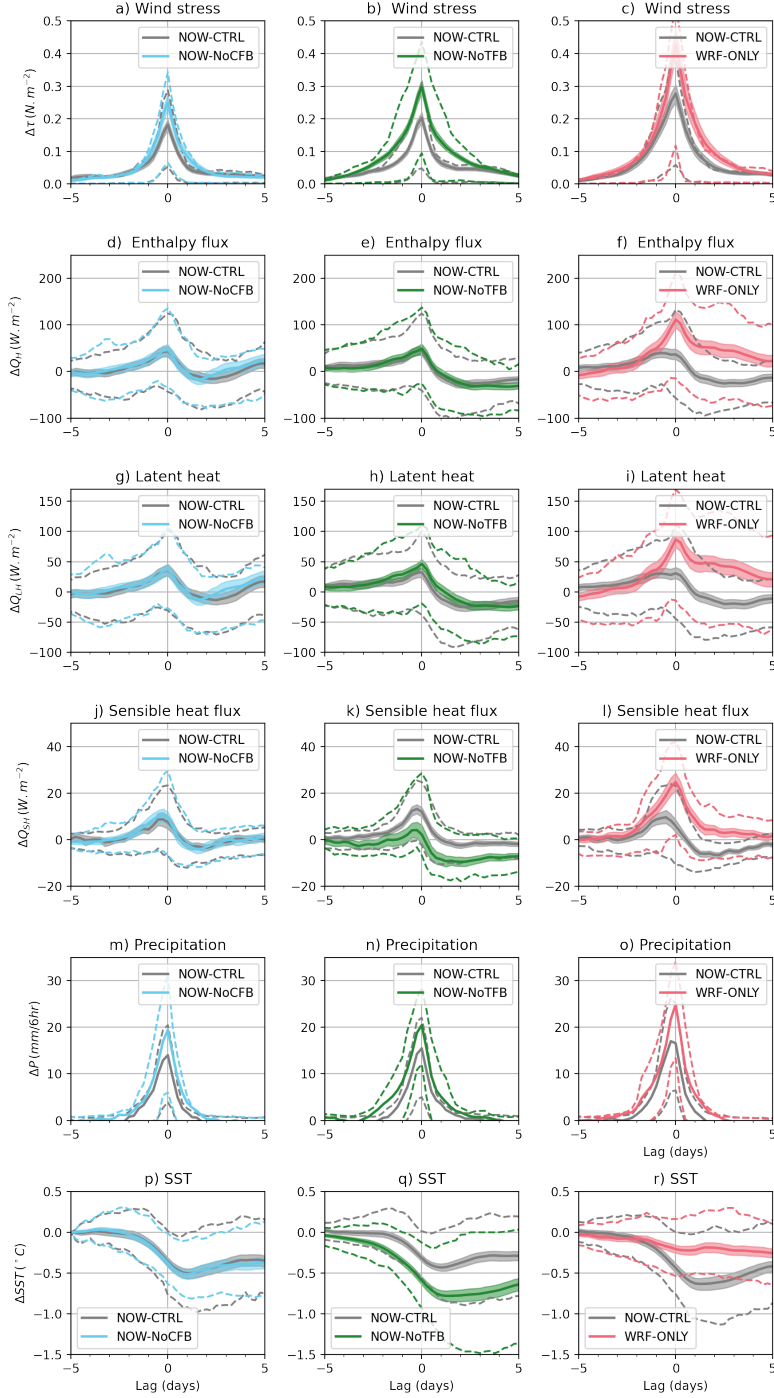


Figure 10. NECL wake composites (warm season, north of $30^{\circ}S$) as a function of time relative to the 5-10 day average prior to the passing of the NECL for: a-c) wind stress τ , d-f) upward enthalpy flux ΔQ_H (latent + sensible), g-i) upward latent heat flux ΔQ_{LH} , j-l) upward latent heat flux ΔQ_{LH} , m-o) total precipitation ΔP and p-r) SST ΔT). Only common events are used to compute the composites for the NOW-CTRL simulation (grey lines) and the sensitivity simulations (coloured lines); the 25% and 75% percentiles of the cyclone distribution (dashed lines) and confidence intervals (coloured shading) at 5% and 95% are estimated using a bootstrap method. The composites are integrated within a 200 km radius.